AD-A018 983

MAGNETO-OPTIC LASER BEAM STEERING

T. R. Johansen, et al

Sperry Univac

Prepared for:

Air Force Avionics Laboratory

October 1975

AFAL-TR-75-122

FG

MAGNETO-OPTIC LASER BEAM STEERING

SPERRY UNIVAC

OCTOBER 1975

TECHNICAL REPORT AFAL-TR-75-122
SUMMARY REPORT FOR PERIOD MARCH 1974 – MARCH 1975

Approved for public release; distribution unlimited

AIR FORCE AVIONICS LABORATORY
AIR FORCE WRIGHT AERONAUTICAL LABORATORIES
Air Force Systems Command
Wright-Patterson Air Force Base, Ohio 45433

UNCLASSIFIED

SECURITY CLASSIFICATION OF THIS PAGE *(When Data Entered)*

REPORT DOCUMENTATION PAGE		READ INSTRUCTIONS BEFORE COMPLETING FORM
1. REPORT NUMBER AFAL-TR-75-122	2. GOVT ACCESSION NO.	3. RECIPIENT'S CATALOG NUMBER
4. TITLE *(and Subtitle)* MAGNETO-OPTIC LASER BEAM STEERING		5. TYPE OF REPORT & PERIOD COVERED Technical 1 March 74 – 1 March 75 6. PERFORMING ORG. REPORT NUMBER
7. AUTHOR(s) T. R. Johansen, P. G. Hewitt, J. Krawczak, and E. J. Torok		8. CONTRACT OR GRANT NUMBER(s) F33615-74-C-1035
9. PERFORMING ORGANIZATION NAME AND ADDRESS Sperry Univac St. Paul, Minnesota 55165		10. PROGRAM ELEMENT, PROJECT, TASK AREA & WORK UNIT NUMBERS Project 2001 Task 02
11. CONTROLLING OFFICE NAME AND ADDRESS Air Force Avionics Laboratory AFAL/TEO Wright-Patterson AFB, Ohio 45433		12. REPORT DATE October 1975 13. NUMBER OF PAGES 74
14. MONITORING AGENCY NAME & ADDRESS*(if different from Controlling Office)*		15. SECURITY CLASS. *(of this report)* U 15a. DECLASSIFICATION DOWNGRADING SCHEDULE

16. DISTRIBUTION STATEMENT *(of this Report)*

Approved for public release; distribution unlimited.

17. DISTRIBUTION STATEMENT *(of the abstract entered in Block 20, if different from Report)*

18. SUPPLEMENTARY NOTES

19. KEY WORDS *(Continue on reverse side if necessary and identify by block number)*

Magneto-optic laser beam steering
Bismuth Substituted rare earth iron garnet

20. ABSTRACT *(Continue on reverse side if necessary and identify by block number)*

An effort to apply magneto-optic laser beam steering to laser recording has been conducted. The approach is based on diffraction of laser beams by stripe domains which exist in bismuth ytterbium iron garnet crystals (BiYbIG). The preparation of BiYbIG crystals by liquid phase epitaxy is complicated by a surprisingly large thermal expansivity of the bismuth substituted garnet. Special substrates, graded interfaces, top seeded rods, bulk crystals, and LPE on very thin (10 μm) substrates were tested as a means of crystal fabrication. LPE on very thin substrates

DD FORM 1 JAN 73 1473 EDITION OF 1 NOV 65 IS OBSOLETE

UNCLASSIFIED

SECURITY CLASSIFICATION OF THIS PAGE *(When Data Entered)*

appears to be the single best short term approach. With this method, lead free, crack free, high bismuth content garnets were for the first time grown by liquid phase epitaxy.

At this time, high inductance ($\sim 400\ \mu H$) drive coils are required to generate the drive field. An azimuth scan uses a resonant circuit but requires a 25-30 0e field for scan initiation and so wastes spots. The radial scan uses all of the spots but requires a broad band drive circuit which limits the number of lines available at 30 frames per sec. When LPE BiYbIG crystals are prepared free of misfit dislocations by making the in-plane lattice match perfect, then the drive requirements will be reduced, and then all of the device goals of the laser recording application can be met or surpassed with the magneto-optic beam steering approach.

FOREWORD

This report was prepared by Sperry Univac, Applied Physics Laboratory, Univac Park, St. Paul, Minnesota under Project Number 2001, Task Number 02, Contract Number F33615-74-C-1035. The work was administered by the Air Force Avionics Laboratory, Air Force Wright Aeronautical Laboratories, with Mr. Leslie J. Lawrence, AFAL/TEO as Project Administrator.

This summary report covers research conducted from 1 February 1974 through 1 March 1975 in the Applied Physics Laboratory, A.D. Kaske, manager. Members of the laboratory personnel who participated are: T. R. Johansen, E. J. Torok, J. Krawczak, F. Hewitt, G. Nelson, D. Fleming, and F. W. Simon. The report is submitted by the authors in May 1975.

This technical report has been reviewed and is approved for publication.

William A. Wallace

WILLIAM A. WALLACE, Major, USAF
Chief, Electro-Optics Technology Branch
Electronic Technology Division

TABLE OF CONTENTS

LIST OF ILLUSTRATIONS

LIST OF ILLUSTRATIONS (CONT)

NOTICE

When Government drawings, specifications, or other data are used for any purpose other than in connection with a definitely related Government procurement operation, the United States Government thereby incurs no responsibility nor any obligation whatsoever; and the fact that the government may have formulated, furnished, or in any way supplied the said drawings, specifications, or other data, is not to be regarded by implication or otherwise as in any manner licensing the holder or any other person or corporation, or conveying any rights or permission to manufacture, use, or sell any patented invention that may in any way be related thereto.

This report has been reviewed by the Information Office (OI) and is releasable to the National Technical Information Service (NTIS). At NTIS, it will be available to the general public, including foreign nations.

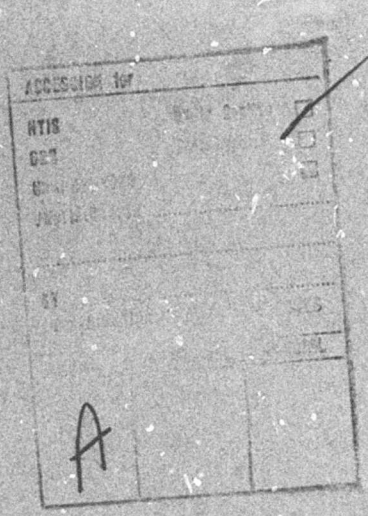

Copies of this report should not be returned unless return is required by security considerations, contractual obligations, or notice on a specific document.

SECTION I
INTRODUCTION

Following the discovery and development of the laser, applications which utilize the brightness and collimation of laser beams have proliferated. Many of the applications require wide angle, high resolution laser beam steering. One such application is laser recording. The effort under this contract is to develop a magneto-optic laser beam steering device which can be used in a laser recording application. The device goal is that an 875 line, 1000 spot, 30 frame/sec raster is to be generated with low drive power and enough optical efficiency to allow recording on 3414 film with moderate laser beam power. The concept of magneto-optic laser beam steering has been demonstrated during work sponsored mainly by two previous United States Air Force contracts (F33615-72-C-1083 and F33615-73-C-1035), and the results are found in the Final Reports.[1,2]

Following a brief description of magneto-optic laser beam steering, the work performed for this contract is described. The two main tasks are: 1) preparation of the stripe domain BRIG, (Bismuth substituted rare earth iron garnet), crystal and 2) design and fabrication of the drive electronics.

A magneto-optic light deflector based on the stripe domain phenomenon is inherently a wide angle, two dimensional, high resolution deflector. Diffraction of a light beam occurs as a result of a periodic variation in the wave amplitude or phase across a wave normal surface. Magnetic stripe domains can introduce a periodic 180° phase variation in a light beam. Consider an array of stripe domains in a magnetic platelet and a light beam propagating normal to the platelet, Figure 1. A stripe domain is a long, straight region of uniform width in which the magnetization vector is nearly constant. In an array of parallel stripe domains the magnetization in every domain has one component which is in the plane of the platelet and parallel to the stripe direction (see Figure 1, where the domains are parallel to the x-axis). This component has a constant magnitude everywhere in the array and causes the stripes to line up with the applied magnetic field. The other magnetization component

---

[1] Technical Report AFAL-TR-72-396 (March 1973)

[2] Technical Report AFAL-TR-74-183 (September 1974)

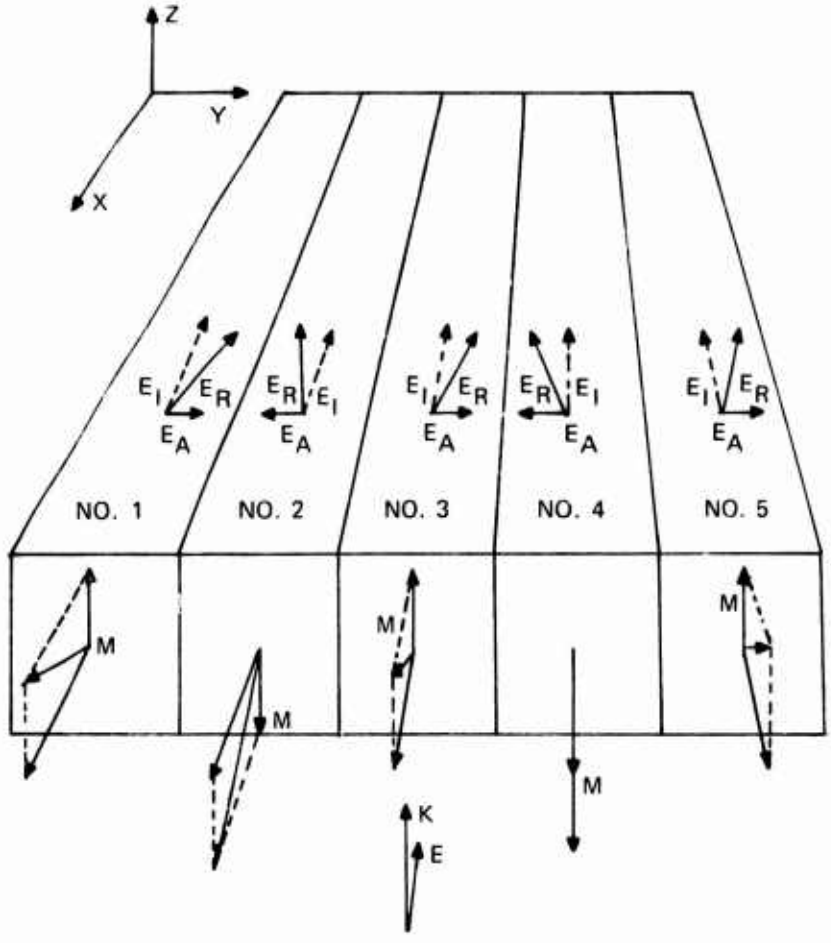

Figure 1. Stripe domains in a platelet. One component of magnetization, M, points out of the plane in the odd-numbered domains and into the plane in the even-numbered domains. Light propagates upward with a wave vector K perpendicular to the platelet and is rotated clockwise (with respect to K) in even-numbered domains and counter clockwise in odd-numbered domains. The rotated optical electric vector is E_R; the initial is E_I, and the alternating component is E_A.

which is normal to the plane of the platelet introduces the periodic phase variation in the light beam. This component points parallel to the z-axis in the odd numbered domains and the opposite way, antiparallel to the z-axis in the even-numbered domains (see Figure 1). Since the sense of the magneto-optic polarization rotation depends on whether the light propagates parallel or antiparallel to the magnetization, this arrangement produces a differential Faraday rotation between light passing through the even-numbered domains and the light passing through the odd-numbered domains. The differentially rotated light beam has an electric component which is orthogonal to the incident electric vector polarization and which has 180° alternations (parallel and antiparallel to y axis) which match the periodic domain structure. In the far field region this alternating vector adds constructively at angles θ_n given by $\text{Sin}\ \theta_n = n\ \lambda/2d$ where d is the width of a domain, λ is the light beam wavelength, and n is the order of the beam (n = 0, 1, 3, 5 etc.). The maximum intensity in the diffracted beams is attained when the Faraday rotation is ±90°. In this special case 81% of the light goes into the first order diffracted beams, 9% goes into the third order beam, and so on. Not only do the stripes line up parallel to an applied magnetic field but the stripe width depends inversely on the strength of the applied field. Variations in stripe width of an order of magnitude have been measured. Thus, both the diffraction angle and the diffraction axis can be varied by the applied magnetic field. Consequently, stripe domains can be used as a wide angle, two dimensional light deflector. Changes in diffraction angle of 20° and changes in deflection axis of 360° have been measured with a green (5145 Å) Ar laser line.

The rate at which a stripe domain deflector can scan is the rate at which the stripe domains can be altered. This depends on the intrinsic properties of the stripe domain element, and the rate at which the external magnetic fields used to control the stripes can be changed. There are two basic switching modes for magnetic platelets: wall motion and magnetization rotation. While the speeds of both processes depend on the materials used and the magnitude of the fields applied, the latter process occurs typically in approximately 10 nanoseconds, while the former process takes place in a few microseconds. While either mode is possible with the stripe domain deflector, the wall motion process appears preferable at this point because the electronics for applying the magnetic field are simpler, and because the extra speed of the rotation process is not required for the applications anticipated.

The efficiency of the deflector can be dramatically improved by using the high figure of merit garnets. The efficiency vs wavelength is shown for various materials in Figure 2. The original 1.06 μm material was YIG. The efficiency is about .14 at room temp and about .8 for YIG at 77°K. The value for YIG shown in Figure 2 is lower than this but reasonable since the efficiency depends on the exact location of the absorption band edge. The efficiency of Gd_2 bi Fe_5 O_{12} is over .8 for a broad range of wavelengths at room temp. Furthermore, the high rotation allows the use of platelets which are about 300 μm thick for single pass operation and which are about 30 μm thick in multiple pass configuration. The efficiency of $Bi_{.7}Y_{2.3}Fe_5$ O_{12} is also quite high. It is expected that by increasing the bismuth content, the efficiency can match that of the Gd garnet. Even at short wavelengths 6328Å, the efficiency is at least 15%.

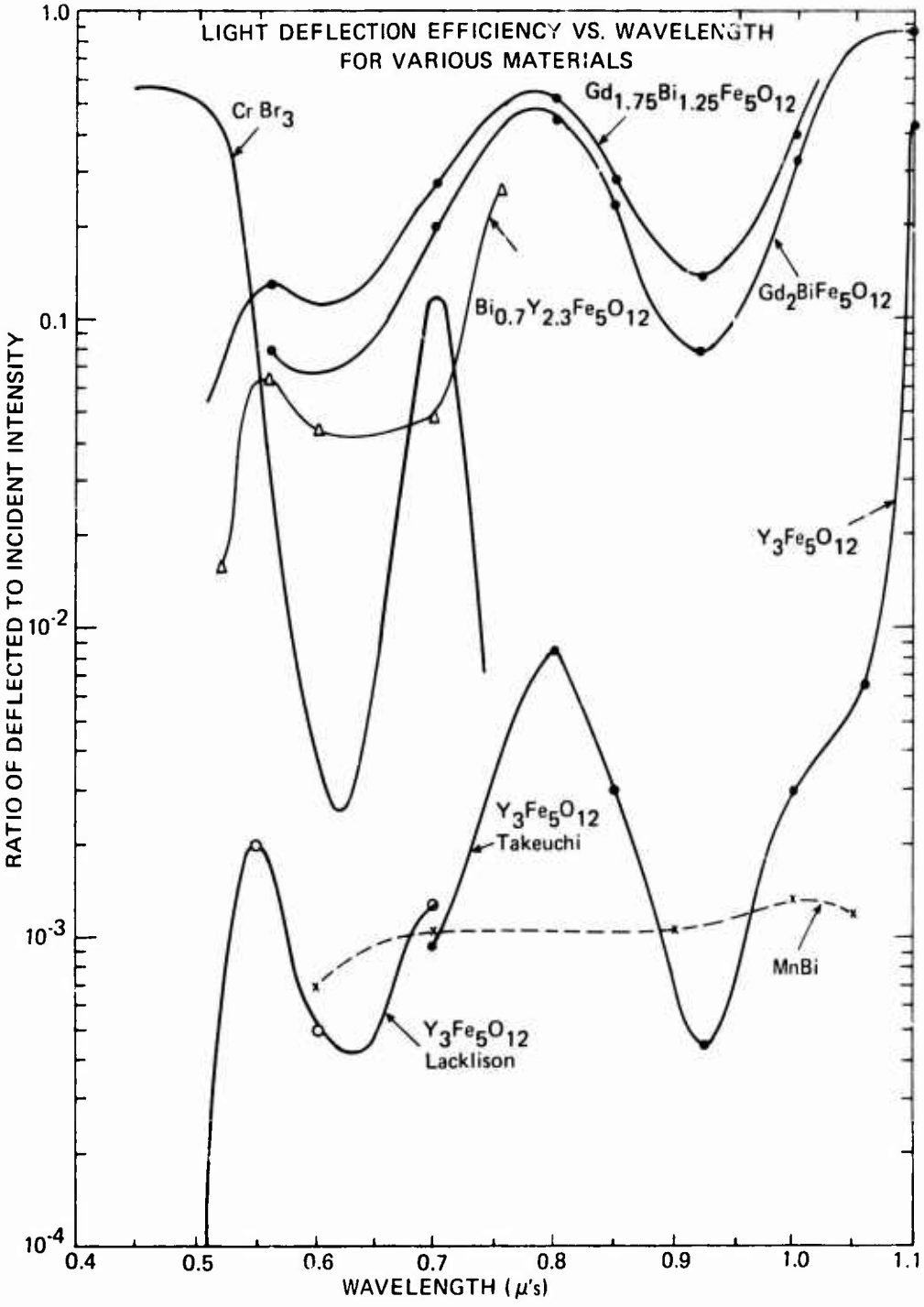

Figure 2. Light Deflection Efficiency vs. Wavelength for Various Materials.

SECTION II
DEFLECTOR CRYSTAL PREPARATION

A. Background

Liquid Phase epitaxy was selected for the method of BRIG deflector crystal preparation on the strength of previous deflector crystal preparation.[1,2] In principle it is the most direct way to obtain planar garnet structures which are optimized for wide angle, high resolution laser beam steering at 6328A. The crystal uniformity and perfection is limited only by the perfection of the substrate crystal and the closeness of substrate to epi-layer lattice match (at temperatures ranging from growth temperature to room temperature), provided that straightforward precautions are observed during substrate preparation and crystal growth. Alternative methods of deflector crystal preparation include slow cooling of a melt for bulk crystals, top-seeded growth at a constant melt temperature, and hydrothermal growth for layers or free crystals.

Prior to the start of this project, epitaxial garnet crystals of BiYbIG had been grown from two distinctly different types of Bi_2O_3 melts: Bi_2O_3, high temperature (900 - 1100°C) melts for which garnet is the precipitate and low temperature (800 - 900°C) melts for which garnet is not the primary precipitate. The high temperature melts produced crystals which were used to determine the lattice constant vs growth temperature curve, Figure 3, for BiYbIG and BiYIG. The low temperature melts always produced crystals which were smoother and had fewer cracks. One would expect on the basis of Figure 3 that epitaxial BiYbIG crystals grown on GGG at temperatures below 1050°C should exhibit a compressive strain since the free lattice constant of such a BiYbIG ought to be larger than the substrate lattice constant. The compressive nature of the strain can be spotted easily by observing the domain structure. What was observed was that the magnetic anisotropy of every crystal grown prior to April 1974 (and every one since) is normal to the film plane. If some of these crystals were under compressive strain the anisotropy ought to be in the plane (or at least some of the crystals should have normal and some should have in plane

---

[1] Technical Report AFAL-TR-72-396 (March 1973)

[2] Technical Report AFAL-TR-74-183 (September 1974)

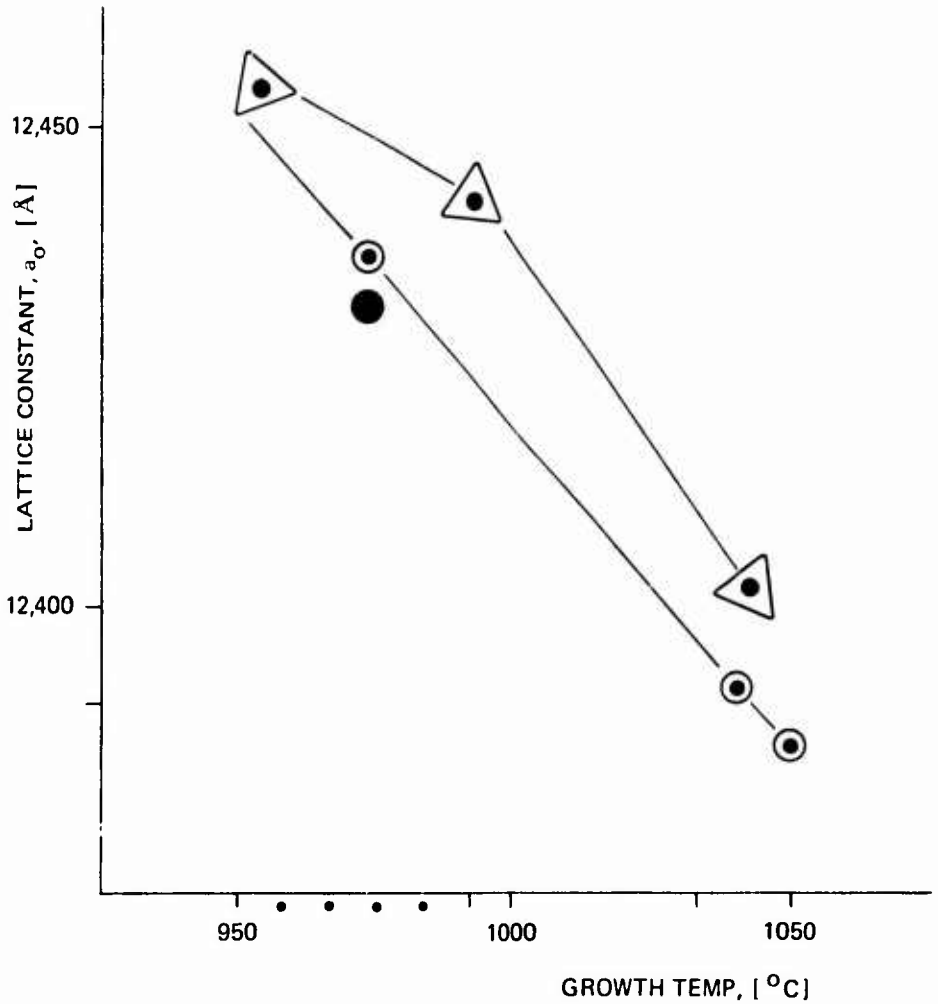

Figure 3. Lattice Constant vs. Growth Temperature for Bi YbIG, (⊙), and Bi YIG (△).

anisotropy). It is assumed that the Bi^{3+} ions do not influence the growth induced anisotropy. Thus, we undertook to measure the thermal expansion rate of the BiYbIG crystals relative to the substrate material.

B. BRIG Thermal Match

The pseudomorphic model[3] for epitaxial garnet crystals shows why garnets such as YIG can be grown on substrates such as GGG in such a way that the strain present in the crystal at room temperature depends only on the lattice match at room temperature. The differential thermal expansion may be off-set by a deliberate lattice mismatch at growth temperature. Hence, when the crystal is cooled to room temperature the differential thermal contraction is compensated by the initial state of strain present at growth temperature. The differential thermal expansion rate (e.g., for YIG on GGG) is small. Typical differential expansion coefficients are 1-2 x 10^{-6} per °K.[3]

A crystal, 421, was selected for the thermal match measurement. It was grown from a low temperature non garnet melt, and is mechanically sound enough to provide x-ray data. The crystal was fixed to a goniometer in such a way that it could be heated to a given temperature while the spacing of the (888) planes was measured. The resolution of this particular single-crystal x-ray technique is about 0.003Å; however, smaller differences can be detected when the peaks are well separated. So, if $\Delta\alpha \sim 1 \times 10^{-6}/°K$, then the film peak would be nearly stationary relative to the substrate peak as the crystal temperature is varied from 22°C to 162°C. Note that in this case $(\Delta\alpha)(\Delta T)\, a_o \sim 0.001$Å. On the other hand, if $\Delta\alpha$ is much larger than 1×10^{-6} then the (888) x-ray peak separation should change as the crystal is heated from 22°C to 162°C. This is exactly what was observed. In Figure 4, $\Delta a^{\perp}$, the lattice difference, $(a_s - a_f)^{\perp}$, in the direction perpendicular ($^{\perp}$), to the crystal plane is plotted vs. crystal temperature. The data shows that $\Delta a^{\perp}$ changed by 0.025Å. A lower bound for $|\Delta\alpha|$ can be derived from this data: $\Delta\alpha \sim -14 \times 10^{-6}/°K$. This is about a factor of 12 different from $\Delta\alpha$ for YIG on GGG.

---

[3]Besser et al, AIP conf Proc No 5, (1971) P 125.

As a check on the instrumentation, $\Delta a^{\perp}$ was measured for several samples of YIG on GGG. Figure 4 shows $\Delta a^{\perp}$ vs. crystal temperature for a CVD YIG crystal (provided by Autonetics) and for a LPE YIG crystal. The agreement of the measured $\Delta\alpha$ and published $\Delta\alpha$ for the CVD YIG crystal is excellent.[3,4,5]

Figure 5 shows data for YIG crystal 609 grown in a PbO melt. While the actual mismatch is large, (0.030 Å), at room temperature, the computed $\Delta\alpha \cong -2.5 \times 10^{-6}$. This compares favorably with a value computed for YIG on the basis of data given by Geller et al.[3,4,5]

Thus the measurement technique is verified with respect to the value of $\Delta\alpha$ computed for BiYbIG. One interpretation of such a large $\Delta\alpha$ is that it is due to the presence of the Bi ions in the crystal. Another cause of the large $\Delta\alpha$ could be platinum contamination in the crystal. An experiment was conducted to probe this question and is described in this section. The measurement was also performed on a BiTm IG crystal grown in a PbO melt: the result is substantially the same.

In order to understand and explain the lattice constant mismatch for the BiYbIG film in Figure 4 it is helpful to consider papers by Besser[3,6] et al and Makino et al[7] on stresses in epitaxial films. In these papers a model is developed to explain film stress and sign in terms of room temperature, lattice constant mismatch and thermal expansion coefficients. The model assumes elastic behavior between room temperature and growth temperature. The model is most applicable when thermal expansion coefficients for the film and substrate are reasonably well matched, e.g., $|\alpha_f - \alpha_s| \leq 1\text{-}2 \times 10^{-6}/°K$. The validity of the model for CVD magnetic oxide films has been demonstrated by ferromagnetic resonance measurements and by observations of magnetic domain structures and film crazing.

In general, the lattice constant of the film will differ from that of the substrate at the growth temperature. For purposes of the model, it is assumed that this

---

[4]Geller et al, J. Appl Cryst (1969) 2, 86.

[5]Geller et al, Matl. Res. Bull. Vol 7, PP 1219 - (1972)

[6]Besser et al Mat. Res. Bull. 6, (1971) 1111-1124)

[7]Makino et al AIP Conf Proc. No 18, (1973) 80

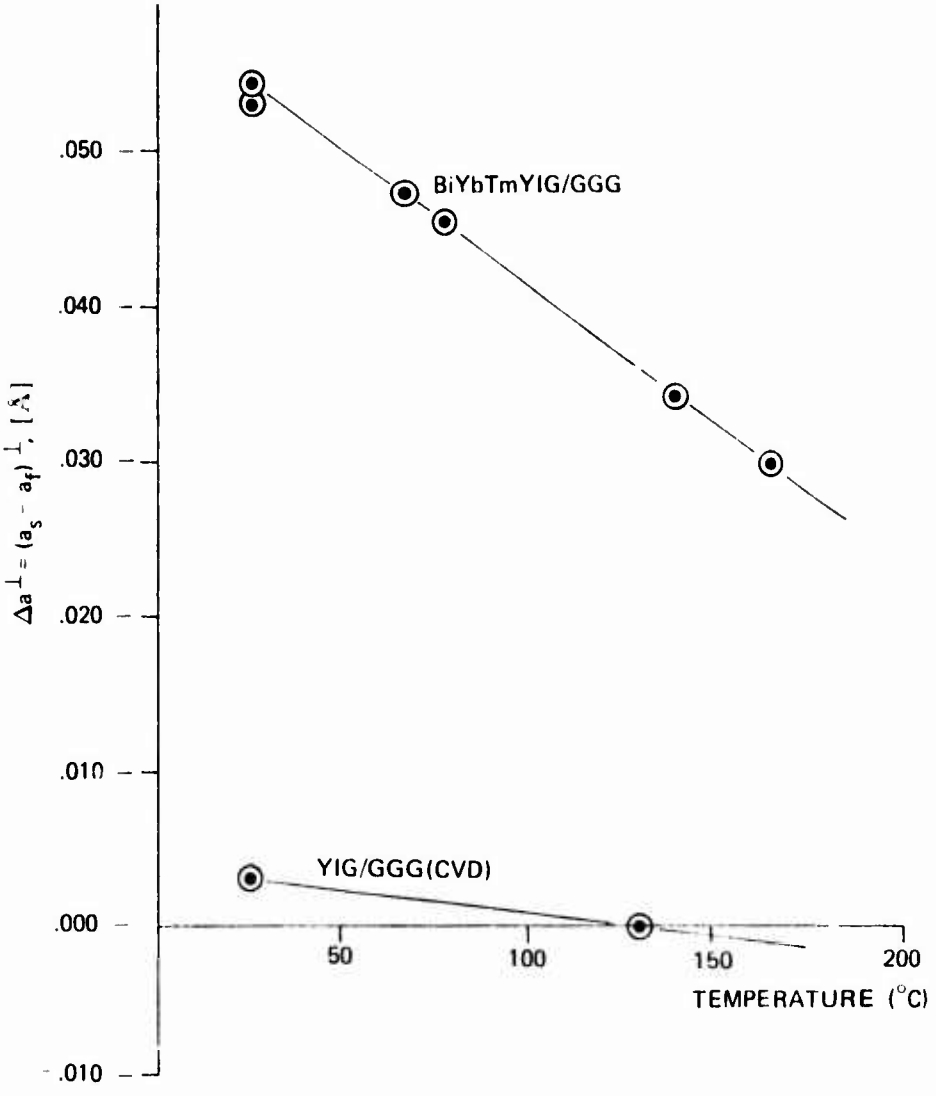

Figure 4. Lattice Match for BiYbTmYIG Relative to GGG and for YIG(CVD) Relative to GGG vs. Temperature.

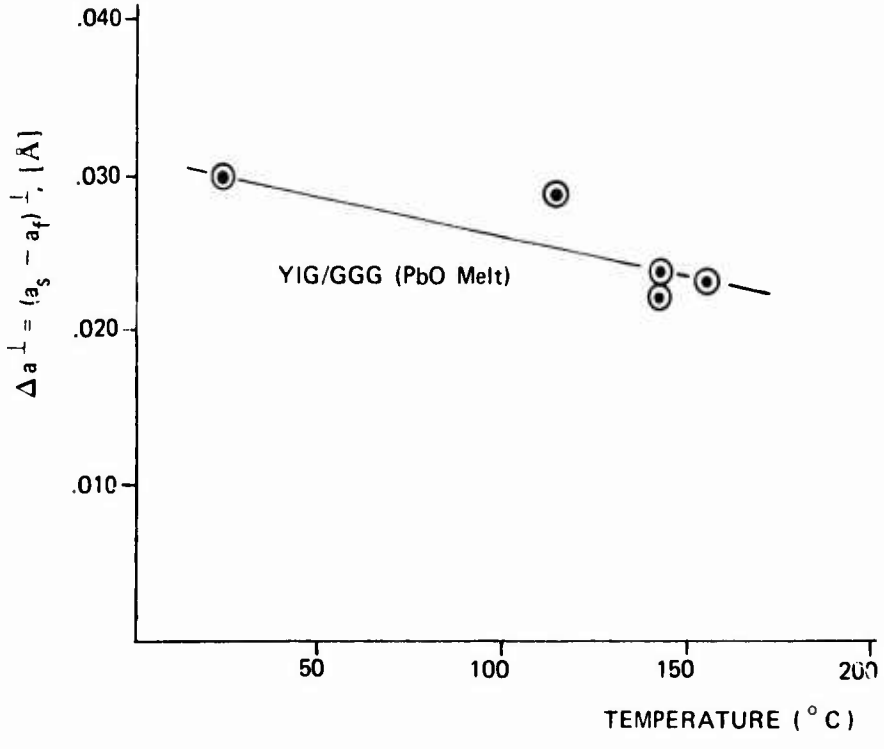

Figure 5. Lattice Match, $\Delta a^{\perp}$, for YIG Relative to GGG vs. Temperature.

mismatch in lattice constants is accommodated in one of two ways. For small values of lattice constant difference, the misfit is assumed to be taken up by the homogeneous elastic deformation of the film so that it fits to the substrate, which is considered to be massive compared to the film so that it does not deform. This range where the lattice mismatch is accommodated by elastic deformation will be referred to as Region I. As the mismatch is increased, limiting values are reached beyond which the stress is relieved by some mechanism, possibly the formation of misfit dislocations at the interface. This second range of lattice mismatch will be referred to as Region II.

In Region I, the stress depends only on the room temperature lattice constant mismatch and is independent of growth temperature. Whereas, in Region II, the stress (and hence the lattice mismatch) is due only to thermal expansion mismatch and is independent of room temperature lattice constant mismatch.

LPE is additionally complicated by the fact that film composition (and therefore room temperature lattice constant and thermal expansivity) can be and frequently are dependent on crystal growth temperature. Even so, the above model for CVD films can be very helpful in understanding the results of LPE film growth.

Another source of mismatch problems could be platinum contamination from the crucible. A crucibleless technique was devised for growing films of BiYbIG. Robbins et al[8] reported that iron garnet films could be grown on gallium garnet substrates by using a coprecipitated slurry. This technique was adapted so that a film could be grown free of any platinum contamination. A micro melt of Bi_2O_3,Fe_2O_3 and Yb_2O_3 was placed on a substrate which in turn was located on a polycrystalline $Bi_1Yb_2Fe_2O_{12}$ pellet. The pile was then lowered into a furnace and the Bi_2O_3 in the micro melt liquified forming a flux that wet the substrate but did not run off the substrate. After a brief growth period the substrate was removed from the furnace. X-ray, thermal expansion data was obtained on one such crystal: the thermal mismatch measured about the same as that of the crucible grown crystals. Thus platinum contamination does not appear to be a significant factor in crystal growth characteristics or mismatch properties.

---

[8]Robbins et al AIP Conf. Proc. No. 5 (1971) 101.

C. Implications of the Large Thermal Mismatch.

It is important that the crystal grows in Region I. This is the only way the domain mobility and uniformity can be optimized. The misfit dislocations generated by Region II growth prevent the formation of a uniform grating and impede the motion of the domain walls. What is the consequence of a large $\Delta\alpha$ for a type I film? Cronemeyer et al[9] and Mathews et al[10] have shown that for films on massive substrates, fractures will occur if the film thickness exceeds the Griffith Crack Length: $hc \cong (1-N)r_o a^2/5\pi(\Delta a)^2$: N = 1/3 is Poissons ratio, $r_o = 3\text{Å}$ is the interatomic spacing, and Δa is the room temperature lattice mismatch. If the crystal grows in Region I, then the match at growth temperature is within .02Å to .05Å.[7] But because of the large differential thermal contraction, the room temperature match $\Delta a \sim (.1 - .02)\text{Å} \sim .08\text{Å}$; for such a film $hc \sim 0.2\ \mu m$. The thickness of the epi-layer cannot exceed hc; so, the epi-layer thickness must be less than 0.2 μm. BRIG deflector crystals of thickness less than 3 μm are not useful.

D. Crystal Preparation Alternatives

The foregoing has shown that simple epitaxy is not possible for the formation of high quality BiYbIG deflector crystals. The following methods were tested as alternatives:

1. Find a modification of BiYbIG with lower thermal expansivity.

2. Modify the GGG or SmGG substrate.

3. Reduce the growth temperature.

4. Abandon LPE in favor of bulk crystals.

While the first alternative is conceptually appealing, the BiYbIG deflector materials requirements already include: 1) high magneto-optic rotation, 2) low

[9]Cronemeyer AIP Conf. Proc., No. 5, (1971) 115

[10]Mathews et al, AIP Conf. Proc., No. 10 Part 1 (1972) p 271

optical absorption, 3) normal anisotropy, 4) high curie temperature, 5) low magnetic coercivity or high wall mobility. To add to this not only the lattice match requirement, but also thermal expansion requirement, is to add to a list that is already long. Nevertheless the possibility should not be ignored.

The second alternative should be probed by adding Bi to the substrate. The ionic radius of Bi^{3+} lies between Pr and Nd and so on the basis of size Bi should substitute into GGG and SmGG. The gallium garnet can be prepared in either bulk or epitaxial form. The epitaxial form is used primarily to obtain an insight into BiGGG properties.

The second approach to substrate modification is the thinning of the substrate such that it is no longer massive compared to the film. Thinning is accomplished either by etching or by mechanical/chemical polishing. The equivalent to a thin substrate is a very massive epitaxial crystal. In the limiting case, a BiYbIG rod, is grown on a substrate seed.

Several methods exist to reduce the growth temperature. PbO -Bi_2O_3-B_2O_3 fluxes can be used for BiRIG crystal growth at temperatures below 700°C. However, until some means exists to prevent the increased optical absorption due to lead inclusion this approach is rejected. Substrate crystals may possibly be prepared in this way. Another possible way to reduce the growth temperature is to use the hydrothermal technique. While this technique has been demonstrated[11,12] for YIG, it remains untried for BiRIG crystals.

The fourth alternative is accomplished by growing via slowly cooling a Bi_2O_3 melt or by using a top seeded ionic salt /B_2O_3 melt. While the Bi_2O_3 melt is known to produce crystals, it would be difficult to obtain large uniform crystals since the change in lattice parameters (see Figure 3) introduced by cooling the melt would cause zoning. The top seeded approach is an isothermal method and so it should be possible, in principle, to avoid the zoning. Of these alternatives each one was tried with the exceptions of BRIG modification and hydrothermal. So far the most

---

[11] Laudise and E. D. Kolb, J. Am. Cer. Soc., Vol. 45, 2 (1962) 51

[12] Ferrand and Daval, J. Cryst Growth 17 (1972) 312

promising method is thinning of GGG substrates. The results of the various approaches will be discussed next.

E. Massive LPE Crystals on Thin Substrates

It has been shown that whenever a massive substrate is used the epitaxial garnet must meet certain lattice match conditions over the entire range of temperature from growth to room temperature. The condition for the differential thermal expansion match can be relaxed if the substrate is not massive with respect to the epi-layer. A massive epi-layer will deform a very thin substrate just as a massive substrate will deform a thin epi-layer.

1. Substrate Thinning

Several methods have been tried in the thinning of substrates: 1) mechanical chemical polishing (Syton, Monsanto), 2) etching in hot phosphoric acid, and 3) ion machining. The main result is that mechanical polishing to 20-40 μm followed by etching in phosphoric heated to 165°-185°C is a quick repeatable way of obtaining substrates 5-10 μm thick.

Pieces of GGG and SmGG substrate material about 600 μm thick and 0.5 to 1.0 cm dia. are attached to steel discs which are in turn attached to a polishing fixture. The substrates are quickly polished with a sequence of coarse 320 through 600 grit papers to 200-300 μm thickness. Syton is used to remove another 100-200 μm. The substrate is then removed from the disc and remounted with the polished side down. Whenever the bonding agent for the substrate pieces does not dissolve easily in warm water or some other solvent, the steel piece itself is dissolved in nitric acid. The process is repeated with only a brief trimming with grit paper. Syton is used to reduce the substrate to 20-40 μm. Several pieces of GGG were thinned to under 10 μm. In all about 30 pieces were thinned to under 40 μm.

In the course of searching for a selective etch to remove GGG from a massive BRIG crystal, substrates were thinned by a hot phosphoric acid etch. Figure 6 shows a curve of etch rate vs. bath temperature for GGG. The etch rate was substantially

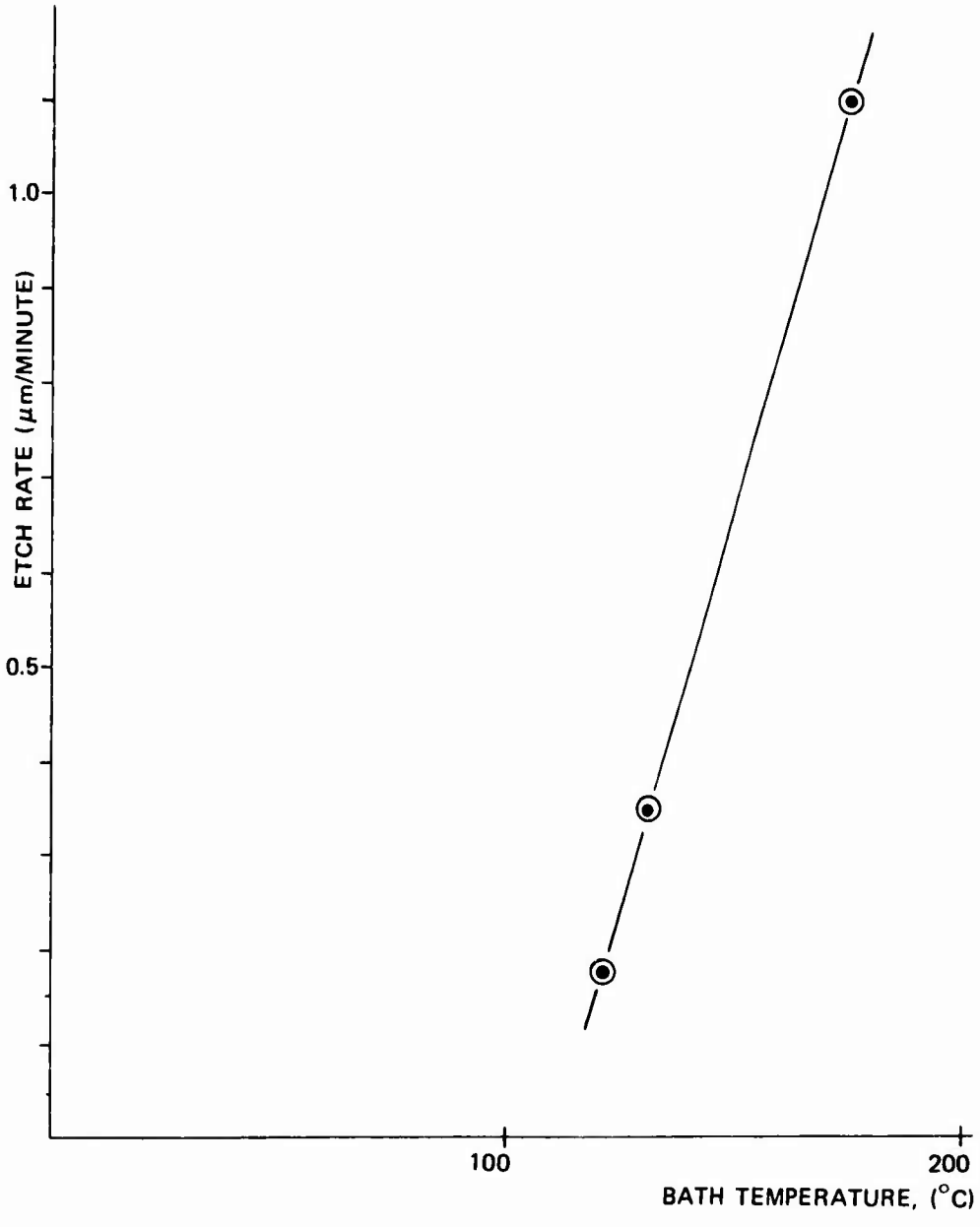

Figure 6. Garnet Etch Rate vs. Bath Temperature. The Bath is Phosphoric Acid.

the same for GGG and BRIG in agreement with Miller[13], the etch used at 175°C is a convenient supplement to Syton polishing. Substrates were etched routinely to 10 μm maximum thickness over the area .5 cm diameter. A piece of 600μm thick GGG was etched to 75 μm thickness. However variation in thickness by ± 25 μm were observed.

The substrate crystals thinned by polishing are not damaged. The phosphoric etch rate is greater[14] for damaged or strained crystals. Thus mechanical defects in polished garnets would show up in the etch treatment. Occasionally scratches were revealed by the etch. Frequently the GGG and SmGG substrates which were supplied by SRC were free of scratches or pits.

2. LPE on Thin Substrates

A number of BRIG crystals have been grown on thin substrates. The main result is that unfractured, sound crystals 2-3 mm across have been obtained. The crystals were grown in a Bi_2O_3-Fe_2O_3-Yb_2O_3 melt with the following proportions .215 moles Bi_2O_3 .100 moles Fe_2O_3 and .07 moles of Yb_2O_3. The growth temperature was varied with changes in the nutrient concentration. The stable phase of this melt is garnet.[2] The growth temperatures ranged from 1040°C to 1090°C. The long growth periods make the high temperature garnet melts more useful than the low temperature non garnet melts[2]. Crystals 75 μm thick were grown at rates of 1-3 μm/min.

The initial crystals were grown on substrates which were ≅ 5 μm thick. Such thin substrates were too delicate to attach to any platinum fixture. The epi-layers were grown by floating the substrate on the melt surface. The upper side of this substrate usually remained bare. Extreme care was required to prevent spontaneously nucleated particles from being trapped beneath the substrate and consequently from being included into the growing crystal.

---

[13]D. C. Miller J. Electron Mtls. Vol 1. 4 (1972)

[14]Electro Chem. Soc. Vol. 120 No. 5 (1973) 678

It became evident that the 5-10 μm substrates are very difficult to handle, and that immersing the substrate is preferred to floating it. So, 20-40 μm substrates were mounted in the immersion fixture, thinned to 10 μm or less in phosphoric acid, and while left in the same fixture, immersed into the melt. This resulted in fewer inclusions, and a better yield of crystals.

3. Statics of BRIG Crystal Films on Thin Substrates

When a film is being grown in a flux at high temperature there is no stress on the film, provided that the lattice constants of the film and substrate match. This match can be accomplished by using an appropriate mixture of large or small rare earth ions in the flux, and by using the proper growth temperature. Thus there should be no cracking during the growth of the film. *Only when such a film is withdrawn and cooled does cracking occur due to thermal mismatch.*

When the film and substrate are withdrawn the bismuth substituted film, which has a larger coefficient of expansion than the substrate, is subjected to tension. Tension on an outside surface causes cracking. An exterior surface can survive a much larger compressive stress than a tensile stress. Tension inside the crystal is tolerable. In fact, "tempered" glass is made by cooling hot glass quickly enough so the outside layer solidifies before the interior. This puts the outer surface of the glass in compression and the interior in tension. Such glass is extremely tough. Thus the problem is to either make a film-substrate combination such that, upon cooling, the exterior film surface is under compression, or at the very least, under very much reduced tension.

The desired goal of making a crystal-substrate combination such that at room temperature the exterior surface of the film is in greatly reduced tension or in compression can be achieved by the use of thin substrates. There are three cases: In the first, film layers are grown on both sides of the substrate (see Figure 7). If the substrate is thin, it will be easily compressed, thus relieving much of the strain of the films. In the second case, a film is grown on only one side of the substrate (see Figure 8). If the substrate is not too large in area, the strain will cause a dish-like deformation. When the substrate thickness is less than twice the film thickness, the exterior surface of the film is in compression. When the substrate thickness is less

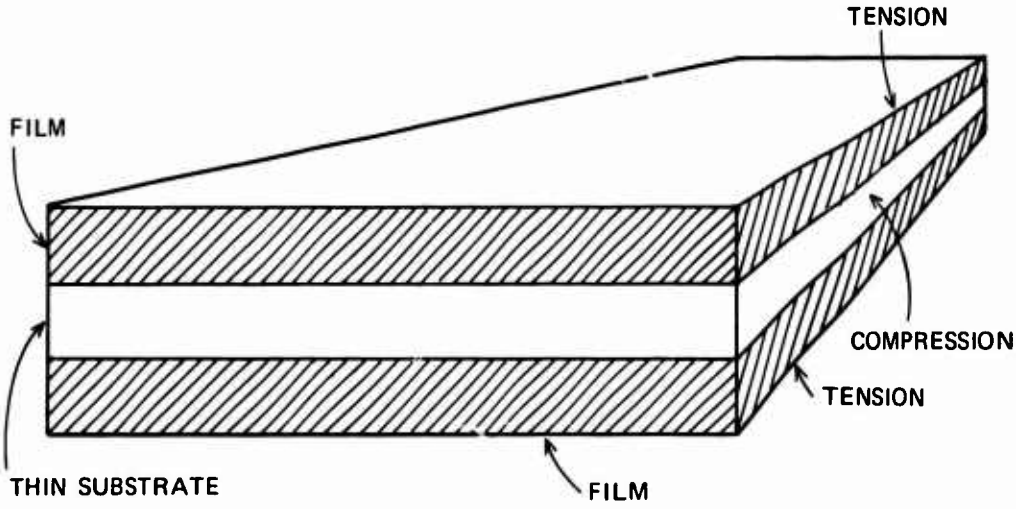

Figure 7. Thin Substrate with LPE Films Grown on both Surfaces.

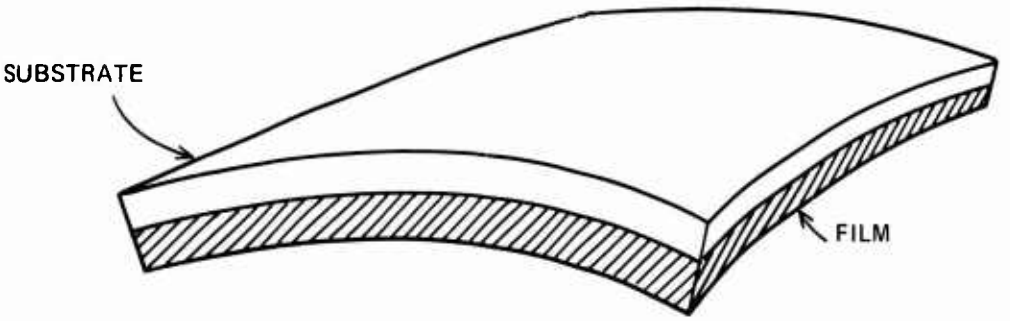

Figure 8. Greatly Exaggerated Drawing of a Thin Substrate with LPE Film Grown on one Surface.

than half the film thickness, the exterior surface of the substrate is in compression as well. In the third case, a film is sandwiched between two substrates of equal thickness (see Figure 9). This is done by first depositing a film on a thin substrate, one side of which is covered by a thin vacuum deposited platinum layer. The film and substrate are then removed from the melt and without cooling, placed in a second melt in the same furnace. Here a layer of substrate material (GGG or SmGG) is deposited. When the film, sandwiched between the two layers, is removed and cooled, all exterior surfaces are under compression.

The second method has been tried with success. Crack free films 25 μm thick have been grown on substrates ranging from 10 μm thick to 25 μ thick. However, the most promising method is the third one. It has the advantages of an unbent film in which the strain is uniform throughout and of being coated with substrate material to which the flux does not adhere.

When films are grown by LPE on both sides of a substrate, and then cooled, both substrates and film will deform without bending due to the difference in thermal expansion coefficients. Define the following symbols:

Let T = room temperature
T_o = growth temperature
σ_f = stress in film
σ_s = stress in substrate
α_f = coefficient of expansion in film
α_s = coefficient of expansion in substrate
E = Young's modulus of film and substrate
h_f = thickness of film
h_s = thickness of substrate
s_f = strain in film
s_s = strain in substrate
s_o = $s_f - s_s$ at growth temperature

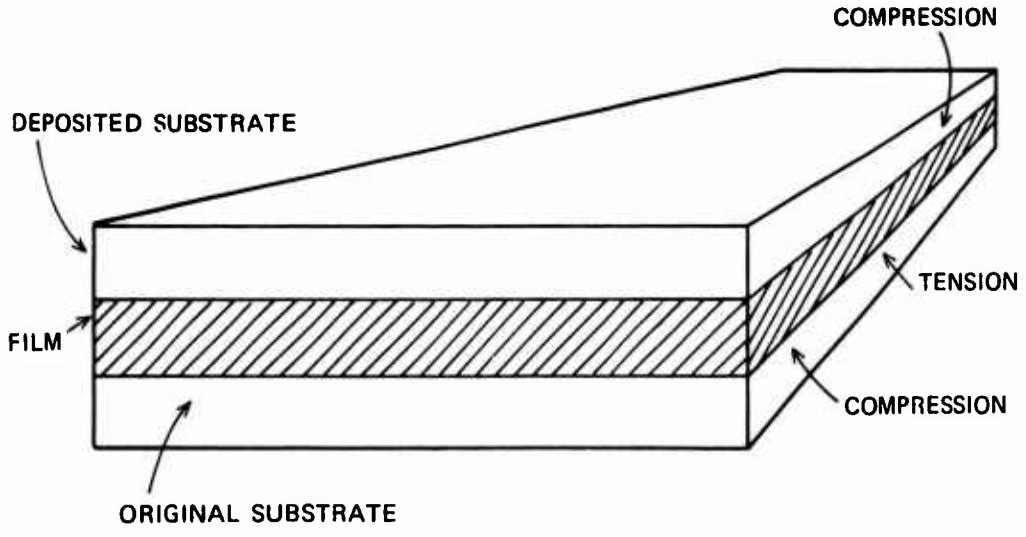

Figure 9. Thin Film Sandwiched between Two Layers of Substrate Material.

The Young's moduli of both garnets (film and substrate) are assumed to be the same. The first equation follows from the definition of the coefficient of expansion:

$$S_f - S_s = (\alpha_f - \alpha_s)(T - T_o) + S_o \qquad (1)$$

This equation is true even if the film and substrate are stretched by external forces. The term S_o arises if the lattice constants of film and substrate are different at growth temperature.

The second equation is a statement that the net sum of all forces on a static body must be zero:

$$2\,\sigma_f h_f + \sigma_s h_s = 0 \qquad (2)$$

The third equation is that the stress is proportional to the strain:

$$\sigma_f = E S_f \text{ and } \sigma_s = E S_s \qquad (3)$$

Equations (1), (2), and (3) are three simultaneous equations that, when solved, yield:

$$S_f = [(\alpha_f - \alpha_s)(T - T_o) + S_o] \; / \; [1 + 2\frac{h_f}{h_s}] \qquad (4)$$

This equation shows the advantage of using a thin substrate. For example, if the film thickness and the substrate thickness are equal ($h_f = h_s$), then the strain of the film is only one third of the value the strain would be if the substrate were very thick.

When only one side of a substrate is covered by a film, the combination will deform when cooled to room temperature. Two types of deformation are possible: a spherical deformation like a saucer and a cylindrical deformation. The former is energetically more favorable for small area substrates and small strains, the latter for large substrates and large strains. The condition for the existence of the spherical

deformation is very roughly that the radius, R of the substrate satisfy the following condition:

$$R < \frac{.2\,(h_s + h_f)}{(\alpha_s - \alpha_f)\,(T - T_o) + S_o} \qquad \text{when } h_s \sim h_f \tag{5}$$

Let us suppose that this condition is met. We wish to calculate the strain in the substrate and film. To do this it is necessary to first calculate the torque in an unbent substrate, and next calculate the amount of bending necessary to generate a compensating torque:

Consider an unbent substrate with a film on one side only. The equilibrium balance of forces is given by the analogue of equation 2:

$$\sigma_f h_f + \sigma_s h_s = 0 \text{ or} \tag{6a}$$

$$S_s h_s + S_f h_f = 0 \tag{6b}$$

These forces form a couple. The torque T_u of that couple about the interface is:

$$T_u = E\left(\frac{S_s h_s^2}{2} - \frac{S_f h_f^2}{2}\right) \tag{7}$$

Since the torque of a couple is independent of the point about which it is measured, this is the torque about the center of the whole film and substrate. Equations 6b and 7 can be combined to yield:

$$T_u = E\,\frac{S_s h_s}{2}\,(h_s + h_f) = -E\,\frac{S_f h_f}{2}\,(h_s + h_f) \tag{8}$$

The next step is to allow the beam to bend; this creates a compensating torque. Let us calculate the magnitude of that torque T_B about the center of the combined film and substrate. At that point we define $Z = 0$ where Z is the distance normal to the film plane. Let the strain at the outside surface due to bending be S_b. Then the strain S^1 due to bending is given by

$$S^1 = \frac{2\,S_b\,Z}{h_s + h_f} \tag{9}$$

The torque due to bending is given by

$$T_B = E \int_{-\frac{1}{2}(h_s + h_f)}^{\frac{1}{2}(h_s + h_f)} S^1 Z dZ \tag{10}$$

The combination of equations 9 and 10 yields

$$T_B = \frac{(h_s + h_f)^2 E S_b}{6} \tag{11}$$

In order for the torques to be balanced, expressions 8 and 11 must be equal:

$$T_u + T_B = 0 \tag{12}$$

The result is

$$S_b = 3 \frac{S_f h_f}{h_s + h_f} = -3 \frac{S_s h_s}{h_s + h_f} \tag{13}$$

The total torque on the exterior substrate surface is:

$$S_b + S_s = S_s \left[1 - \frac{3 h_s}{h_s + h_f} \right] \tag{14}$$

The total torque on the exterior film surface is:

$$S_f - S_b = S_f \left[1 - \frac{3 h_f}{h_s + h_f} \right] \tag{15}$$

where, for the film on one side of the substrate only, S_f is given by the analogue of equation 4:

$$S_f = \frac{(\alpha_f - \alpha_s)(T - T_o) + S_o}{1 + \frac{h_f}{h_s}} \tag{16}$$

Equations 14 and 15 are plotted in Figure 10. It shows the strain at the surfaces of a bent film as a function of fractional substrate thickness. Figure 10 shows that the strain at either surface can be either compressive or tensile depending

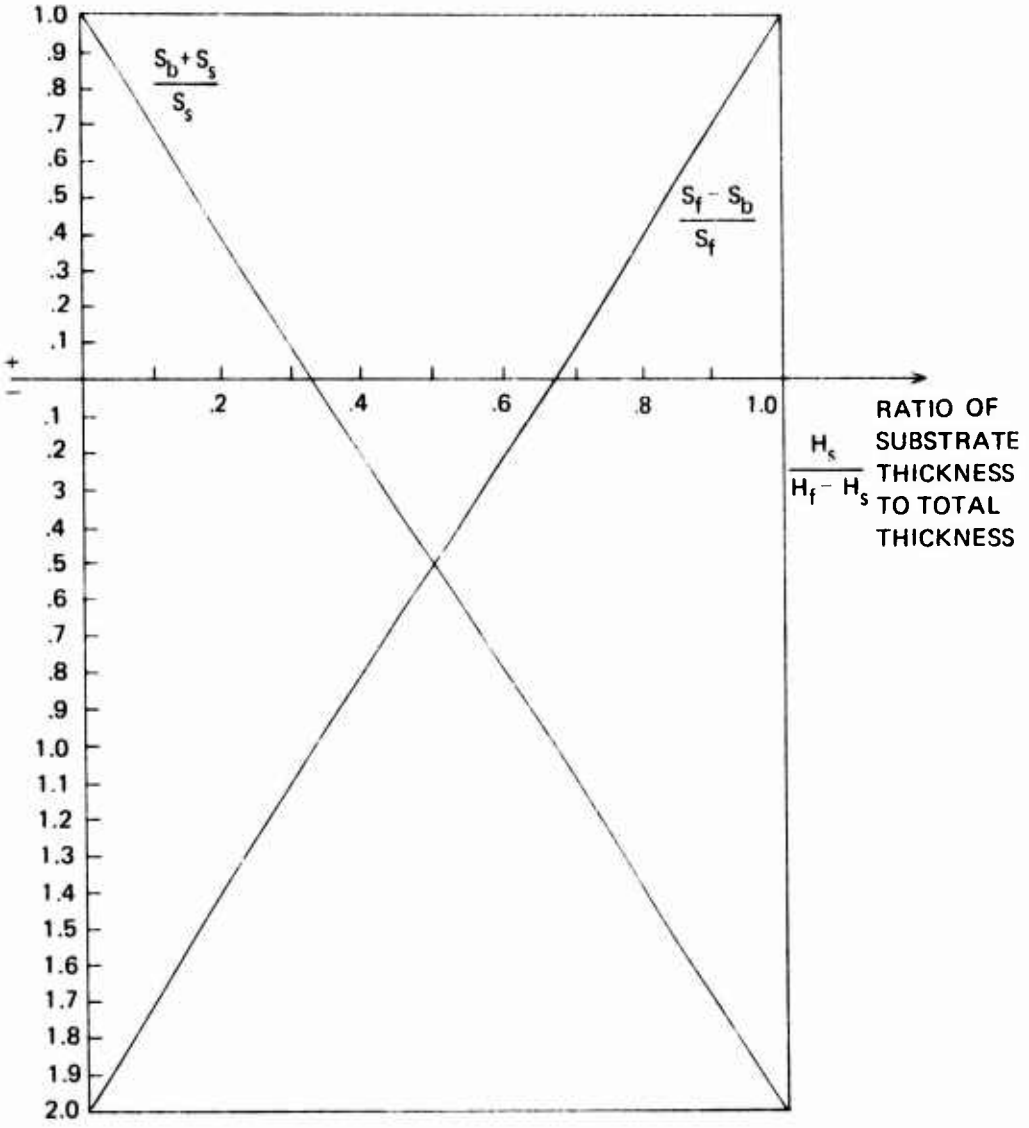

Figure 10. Ratio of Strain at the Surfaces of a Bent Substrate to that of an Unbent Substrate as a Function of Fractional Substrate Thickness.

on the relative thickness of film and substrate. The stress at the exterior film surface is tensile if the substrate is more than twice as thick as the film; that stress is compressive if the substrate is less than twice as thick as the film. The stress at the exterior substrate surface is tensile if the substrate is more than half as thick as the film; if the substrate is thinner, that stress becomes compressive.

The situation is perhaps easier to understand by referring to Figures 11-15. There the strain throughout the thickness of both film and substrate is plotted for various film and substrate thicknesses. Since cracks originate at the surfaces and not in the interior it is desirable to have a substrate that is less than twice the film thickness; then, any cracks will first appear in the substrate. It is even more desirable to have a substrate that is less than half the film thickness since then both exterior sides are in compression, and should not crack. Experimentally we are growing films about 25 μ thick.

4. Results of Massive Crystal LPE

The crystals grown in this way are characterized as follows: The magneto-optic rotation is 1 - 3 x 10^{4}°/cm. Several crystals have over 45° rotation per pass. All of the crystals have stripe domains. However, the stripes are not of the quality necessary for laser beam steering. The cause for this seems to be Region II growth.

The substrate has been removed from crystals ~ 3mm x3mm. The removal, and with it the removal of the bending strain, does not improve the domain quality substantially. A pronounced hill and valley structure developed during growth on the surface of crystals thicker than 25 μm. The removal of this outermost region improves the domain structure only slightly.

Both the outer and inner sides have been ion machined. This process ought to remove the surface strains and normally does improve the domain wall mobility. The effect of etching a smooth BiYbIG crystal in hot phosphoric acid is to create numerous pits. The BiYbIG crystals so grown are probably grown in Region II.

The hill and valley structure takes the form of (110) faces with rapid growth occurring in the (100) direction (as opposed to the desired (111) direction). This is

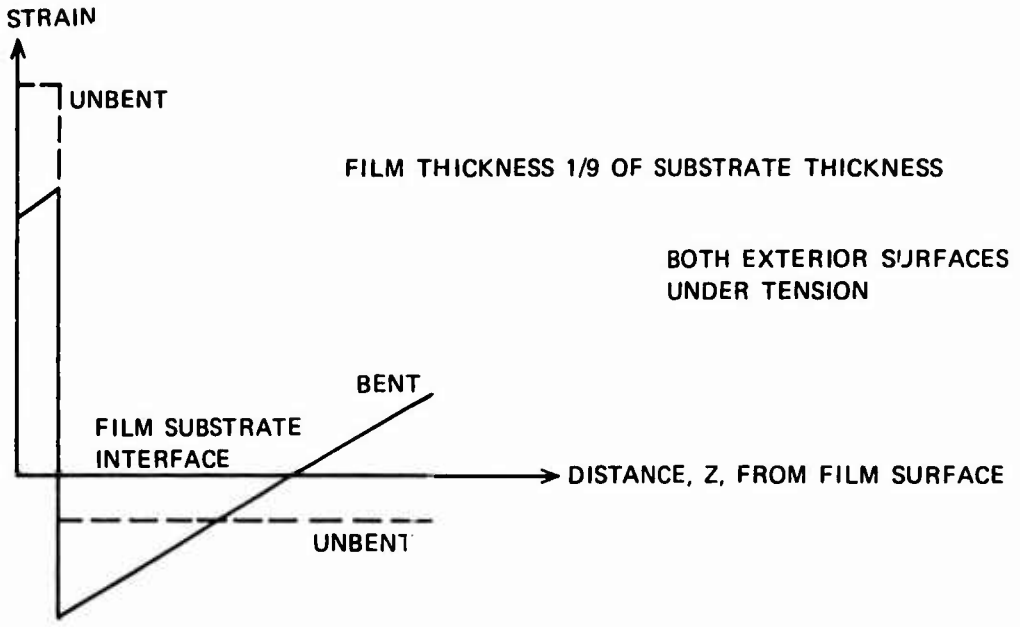

Figure 11. Strain vs. Distance for Film Thickness 1/9 of Substrate Thickness.

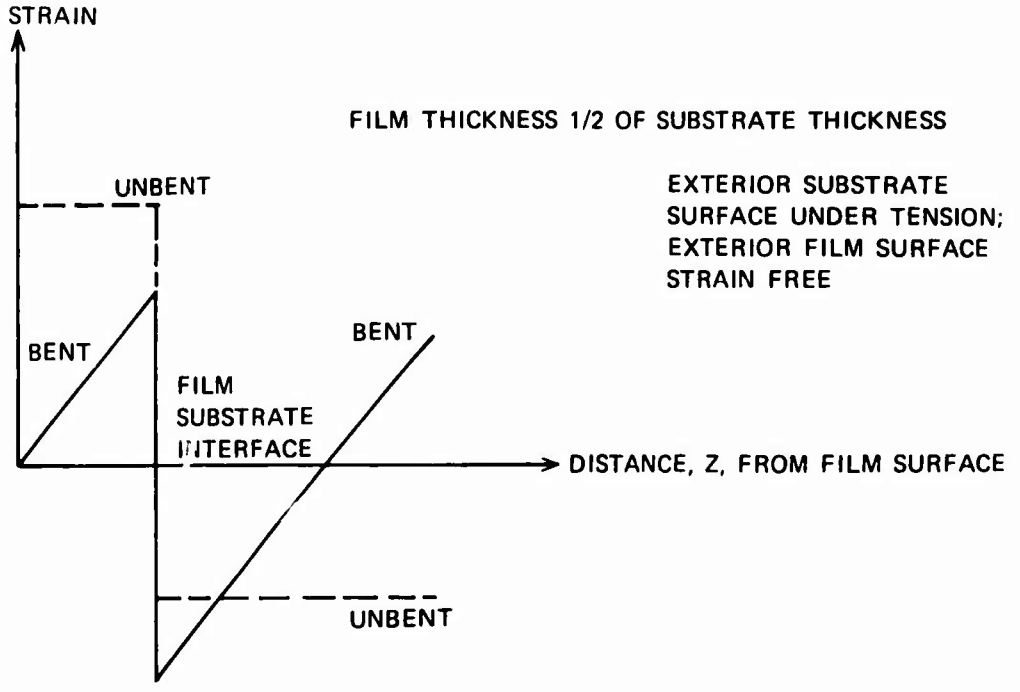

Figure 12. Strain vs. Distance for Film Thickness 1/2 of Substrate Thickness.

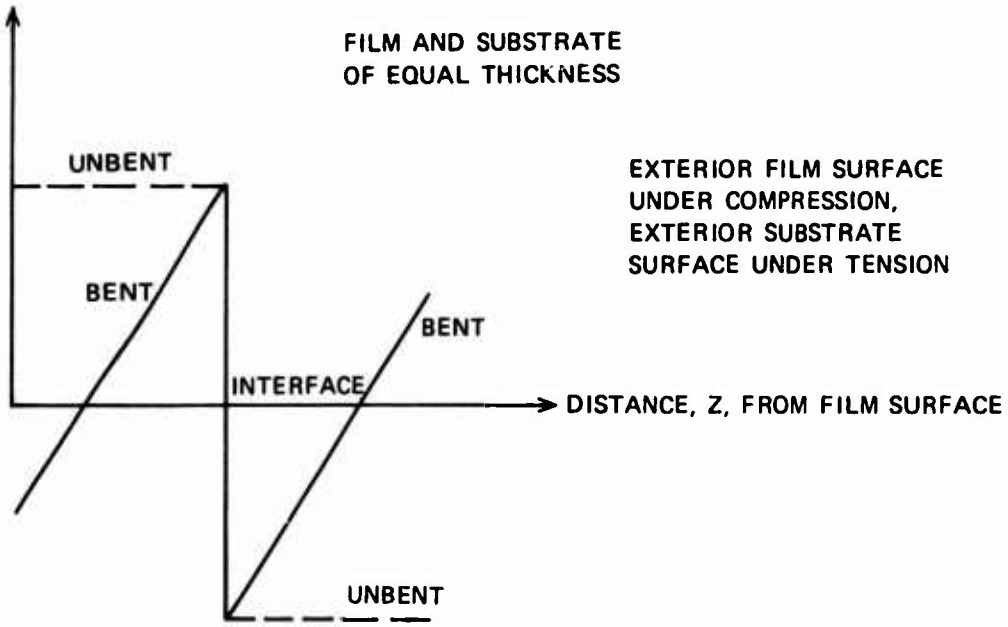

Figure 13. Strain vs Distance for a Film and Substrate of Equal Thickness.

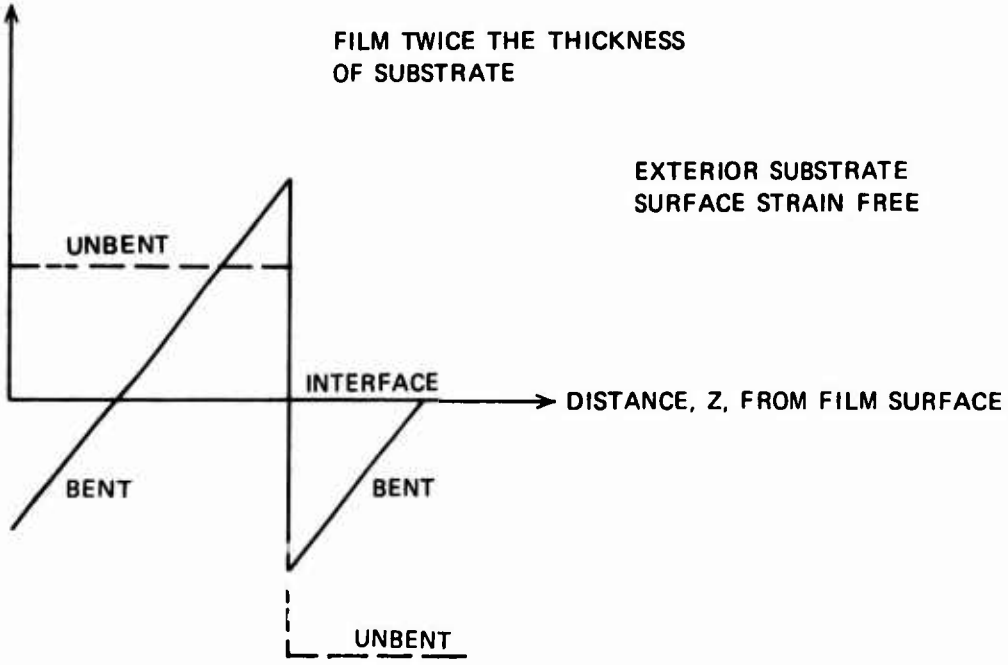

Figure 14. Strain vs Distance for a Film Twice as Thick as the Substrate.

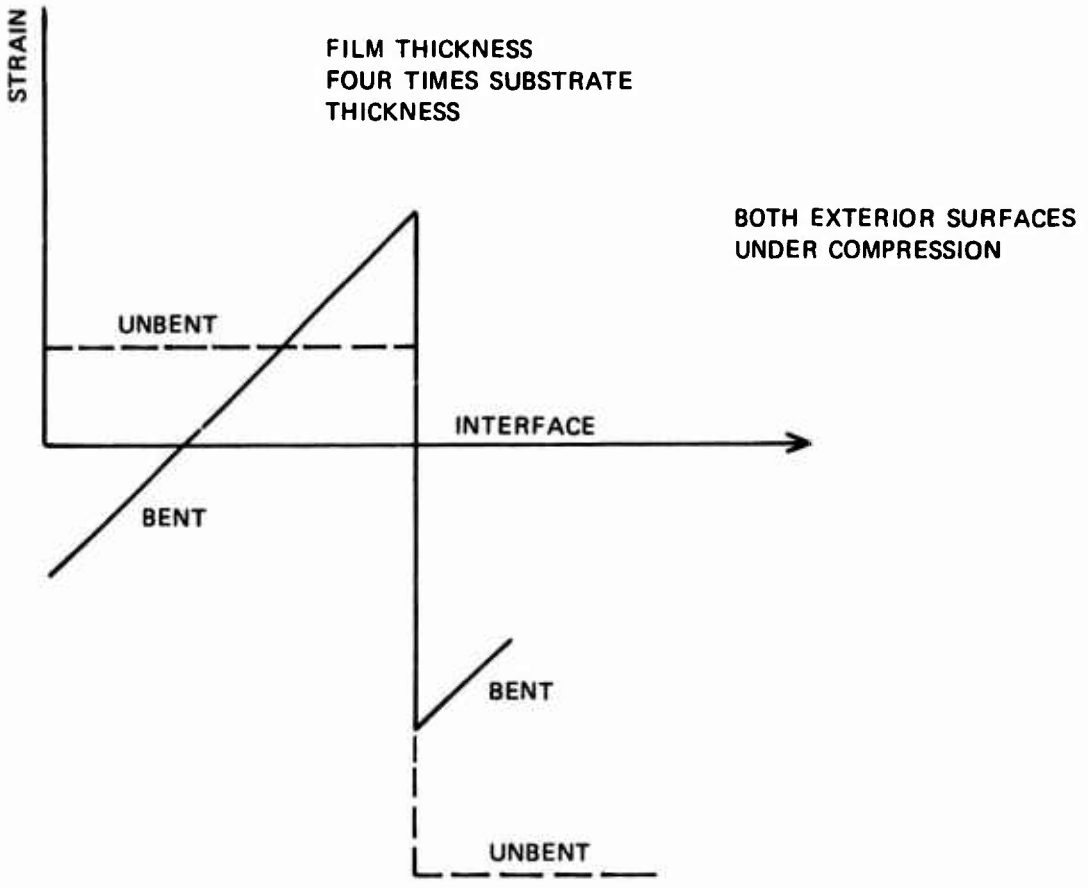

Figure 15. Strain vs Distance for a Film Four Times as Thick as the Substrate.

particularly noticeable on the edges of the substrate where (110) plates grew in (100) directions at rates of 15 μm/min. The plates contain stripe domains and ±45° of rotation was observed in some of these plates.

In summary a method has been devised and demonstrated for preventing epitaxial BRIG fracture. The main advantages of LPE are incorporated into this method: planar, nearly perfect substrate crystals are culled and the substrate crystal prefection is available to the epitaxial crystal. Region I growth must be guaranteed and so in-plane lattice match measurements for these crystals must be obtained.

F. BiGGG Substrates

The use of BiGGG (bismuth substituted) substrates to reduce thermal expansion difficulties was investigated. Sufficient bismuth substitution should increase the lattice constant and thermal expansion coefficient of the substrate and allow for a better film substrate match. These substrates were prepared at Sperry Research Center. The substrates were sliced from bulk crystals grown from a PbO flux. The substrates were polished in our labs. X-ray fluorescence indicated the presence of bismuth in the substrate material.

A BiYbIG crystal was successfully grown on one of the BiGGG substrates. X-ray data for the thermal dependence of the lattice mismatch is shown in Figure 16. A second BiYbIG crystal was grown under identical conditions and its x-ray data is also shown in Figure 16. The similarity of the two curves suggests that the two substrates are not very different. Other x-ray data shows that (contrary to expectation) the lattice constant for the BiGGG substrate is smaller than that for the GGG substrate. Since the slopes of curves are very similar, it would appear that there is not much Bi (which should increase the thermal expansion coefficient) in the BiGGG substrate.

The growth of these two films is probably Region II type where the room temperature film stress is independent of room temperature lattice constant mismatch. For this type of growth the smaller lattice of the substrate should have improved the room temperature lattice constant match, but this was probably more

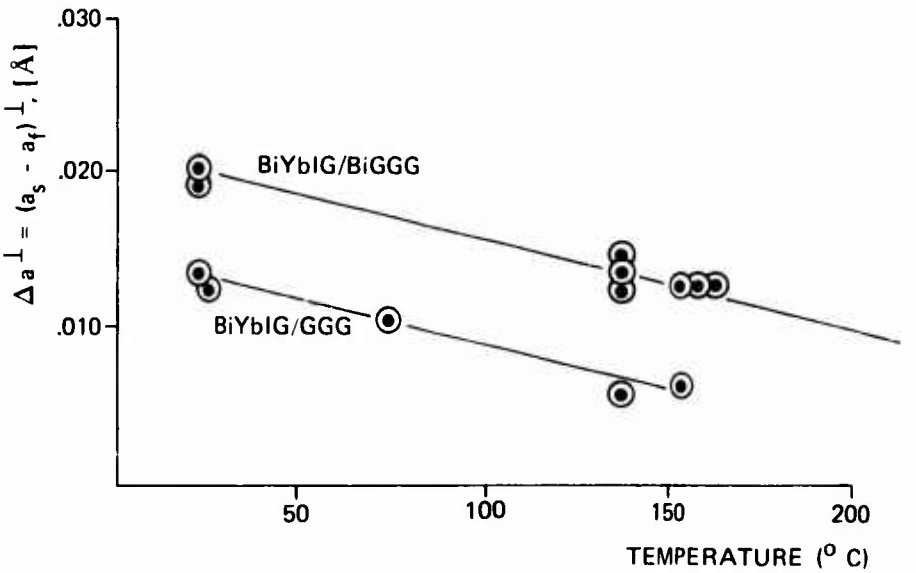

Figure 16. Lattice Match, $\Delta a^{\perp}$, for BiYbIG Relative to a BiGGG Substrate and Relative to a GGG Substrate vs. Temperature.

than compensated for by the increased thermal coefficient of expansion of the BiGGG substrate.

G. Graded Interfaces

Another method investigated to reduce this thermal mismatch problem was the use of a graded interface where intermediate crystal layers are grown to ease the transition from the substrate to the final film layer. Epi-layers of BiYGG and BiGGG were grown in order to 1) determine how to accomplish Bi substitution in a gallium garnet substrate and 2) determine whether epitaxial Bi-Fe garnet crystals can be grown in turn on a graded interface.

Several crystals of $Bi_xY_{3-x}Ga_5O_{12}$ and $Bi_xGd_{3-x}Ga_5O_{12}$ were grown on (111) GGG substrates from a Bi_2O_3 melt containing nearly stoichiometric amounts of Y_2O_3 and Ga_2O_3. X-ray data shows that very little, ($x < .1$), bismuth substituted into these crystals. Upon the suggestion of Dr. Kestigian at Sperry Research Center, an amount of PbO equal to the amount of Bi_2O_3 was added to the Gd melt. Crystals of BiGGG were grown with $x \leq .2$.

X-ray data taken on three of these crystals showed that the lattice constant of the epi-layer was smaller than that of the substrate at room temperature. This is consistent with the bulk grown BiGGG crystals grown at Sperry Research Center. The data also showed that the lattice constant mismatch was independent of both measurement temperature and growth temperature. This is further indication that only a small amount of bismuth went into the film layer, and also indicates that the growth is described by Region I.

In connection with Bi substitution in GGG, Sturge, Blank, and Wolfe[15] have reported on the Nd distribution coefficient in epitaxial YAG. They found that the distribution coefficient is much larger for (110) faces than for (111) faces at certain Nd melt concentrations. What this means is that more Nd substitutes into a (110) YAG epi layer than a (111) YAG epi layer. A similar effect may be causing the low Bi substitutions into our (111) GGG epi-layers.

Several of the BiGGG epi-layers were used as intermediate layer substrates for BiYbIG crystals. Figure 17 shows that the lattice match $\Delta a^{\perp}$ for the BiGGG layer and GGG substrate changes when a BiYbIG layer is grown over the BiGGG layer. The small shift, 0.002Å, which is close to the limit of experimental error, indicates only a slight mechanical relaxation in the BiGGG layer.

Figure 18 shows the thermal dependence of lattice match relative to the GGG substrate for three BiYbIG crystals grown on BiGGG intermediate layers along with a BiYbIG crystal grown directly on the GGG substrate. The slopes of the curves show that all the films have nearly the same coefficient of thermal expansion. The curve for the film grown directly on the GGG substrate does not differ significantly from those grown on the intermediate layer, therefore the intermediate layer does not have a significant effect. The room temperature lattice match of the BiYbIG layer relative to GGG is apparently a function of the growth temperature and is plotted in Figure 19. This curve indicates that the lattice constant of the unstrained film is increasing with growth temperature at a rate of 0.0005Å per °C. This is contrary to previous data where the lattice constant of unstrained crystals was found to decrease with increasing growth temperature (Figure 20). Since the films in Figure 19 were grown at temperatures close to the freezing point, this discrepancy might be due to the strong dependence of viscosity and diffusion rates on temperature. Diffusion rates probably affect crystal composition. In any case, the free crystal lattice constant cannot be determined from the growth temperature. A room temperature lattice constant smaller than the substrate would indicate Region I growth. A room temperature lattice constant larger than the substrate would indicate Region II growth. Growth in either region results in a thermal expansion coefficient of approximately $1.01 \times 10^{-5} C^{\circ -1}$.

---

[15] Sturge, Blank, Wolfe, Mat Res Bull. Vol. 7 989-998 (1972)

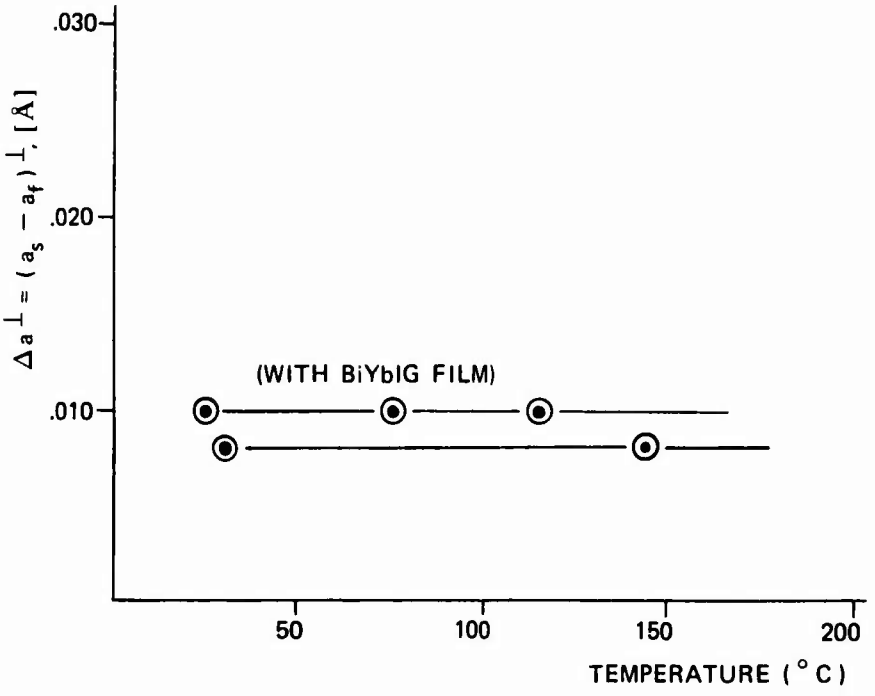

Figure 17. Lattice Match for a BiGGG Intermediate Layer Relative to the GGG Substrate. The BiYbIG Layer Introduces a Small Change in the Lattice Match.

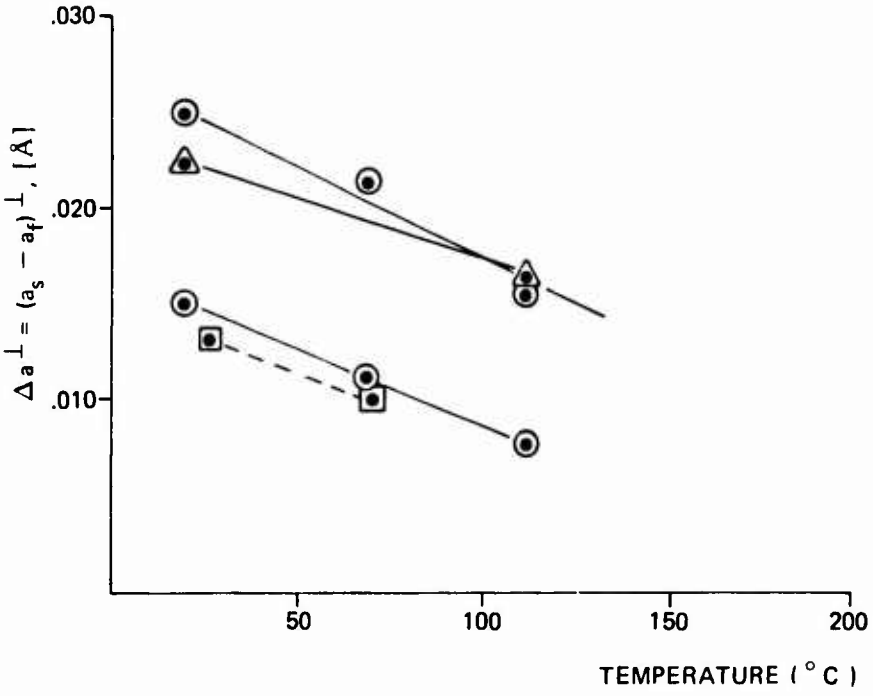

Figure 18. Lattice Match, $\Delta a^{\perp}$, for BiYbIG Relative to the GGG Substrate:

——— With BiGGG Intermediate Layer

- - - - - Without Intermediate Layer

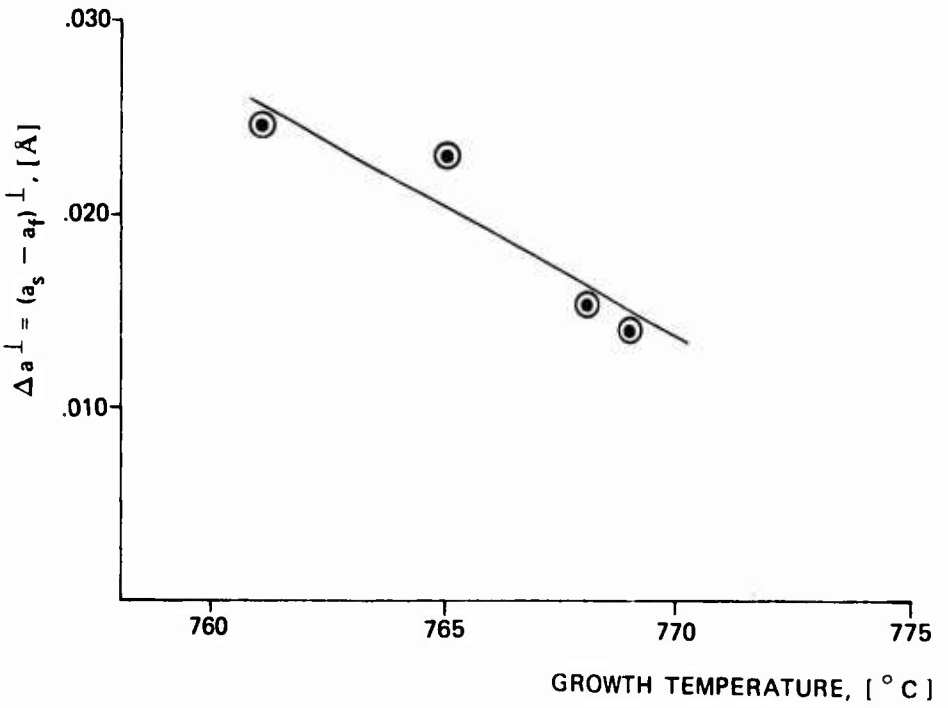

Figure 19. Room Temperature Lattice Match, $\Delta a^{\perp}$, for BiYbIG Relative to GGG. The Crystals were grown at the Melt Freezing Point.

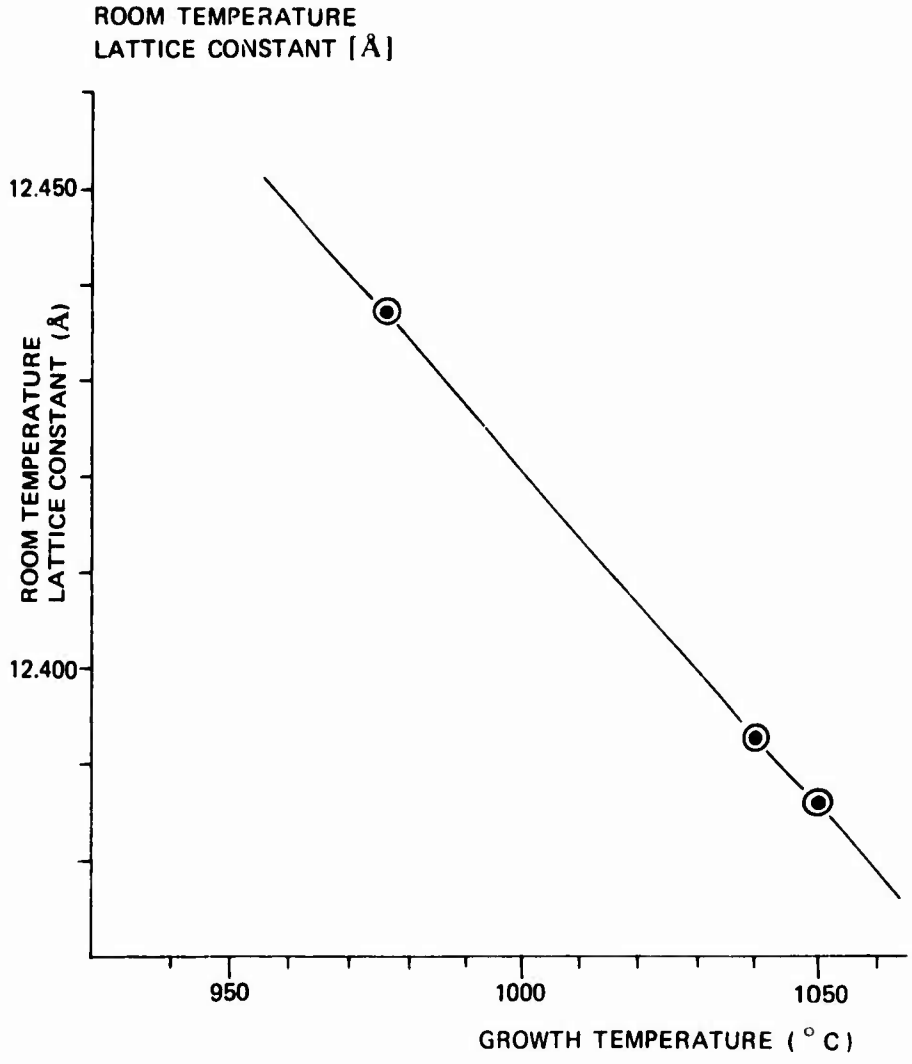

Figure 20. Lattice Constant vs. Growth Temperature for BiYbIG Crystals.

The graded interface system of BiGGG does not appear to solve the thermal match problem. The interface must be grown in Region I and the deflector BiYbIG layer must be grown in Region I. Thus, the substrate lattice will predominate throughout the layers unless mechanical relaxation occurs. The question of how much relaxation is available from the BiGGG system should not be treated until it is possible to substitute more Bi into the layer and thereby obtain thermal properties in the intermediate which are similar to the thermal properties of BiYbIG.

H. Top Seeded BRIG Rods

Lineras[16] and Kestigian[17] have reported the growth of top seeded YIG rods. Their technique employs a $BaO \cdot 0.6B_2O_3$ solvent heated in such a way that the top of the melt where the (isothermal) growth occurs is at least 20°C hotter than the bottom of the melt where solid YIG nutrient is located. The melt is less dense than YIG so any extraneously nucleated crystal sinks to the bottom; furthermore YIG melts congruently in this system[18]. In view of the ease of obtaining rods reported by Lineras and Kestigian it was decided to probe this method to obtain rods of BRIG.

In his 1962 article, Lineras presents a rationale for adjusting the composition of the stable phase by changing the relative amounts of Ba and B in the solvent. The more B, the more Fe in the stable phase. The first question in adapting the top seeded method to BRIG is what happens to the solvent/stable phase relation when Bi_2O_3 is added to the melt? The second question is, can growth occur in such a way (eg., low enough temperature) that a useful amount of Bi goes into the crystal?

Several rods of BiYIG were grown as follows: A solid polycrystalline piece of $Bi_1Y_2Fe_5O_{12}$ garnet was prepared by pressing the mixed oxide powders and firing overnight at 980°C[19]. This poly-crystal was used as a nutrient. The phase diagram of

---

[16]Lineras, J. Appl Phys. 35, 2 (1964) 433-435

[17]Kestigian, J. Am. Ceram. Soc. 50, 3 (1967) 165-166

[18]Lineras, J. Am. Ceram. Soc. 45, 7 (1962) 307-310

[19]Geller, et al, Appl Phys. Lett 3, 2 (1963) 21-22

Levin and McDaniel[20] was used as a guide for adjusting the growth temperature: the solvent contained 41.6 mole % B_2O_3. The largest rod was 6mm dia. and about 6mm long. The period of growth was 7 days. The rod was self seeded on a piece of Pt wire which initially projected about 1mm into the melt. Once nucleation occurred, the wire and growing crystal were raised (manually) about 1mm a day. The growth temperature was 1100°C and the gradient 50° over the 4 cm melt depth.

Thus the growth of crystal BRIG rods can be accomplished via the top seeded technique. The amount of Bi in the rod must be maximized, and this is the next step.

A BiYIG rod was examined via x-ray fluorescence for Bi content. The result is that the Bi peak for the rod is only 0.09 the intensity of the fired material Bi peak. Using a linear approximation, the rod contains only 0.1 Bi per formula. Thus it is imperative that the technique be altered to obtain more Bi. Figure 3 shows that at a given growth temperature more Bi substitutes into the Yb garnet than into the Y garnet. Since it is difficult to grow rods at a temperature lower than 1100°C, it is worthwhile to try a Yb melt to take advantage of the greater rate of substitution.

The difficulty in obtaining the low (~ 980°C) growth temperatures reported by Lineras is that other phases show up. Transparent hexagonal platelets containing Ba, Yb or Y, O, and a trace of B (Arc Spectroscopy) occur when barium rich melts are cooled; barium ferrite crystals occur in boron rich melts. The plates effectively set a lower limit of ~ 1020°C on the growth temperature.

Three other solvent systems were examined as alternatives to barium borate: 1) bismuth borate 2) bismuth barium borate and 3) disodium oxide molybdenum oxide. The bismuth borate system is attractive since Bi_2O_3 dissolves Fe_2O_3 more readily than it dissolves rare-earth oxide as is the case with BaO. Based on the rationale of Lineras (J Am Cer Soc 1962), B_2O_3 should be added to make iron garnet the stable phase. To this end the Bi_2O_3-B_2O_3 system was checked. The phase diagram of Levin and McDaniel[20] resembles the BaO-B_2O_3 system in that it contains a series of eutectics, the lowest occurring at 20 mole % B_2O_3 and 622°C.

---

[20]Levin et al, Phase Dia. Ceram., Am Cer Society 1964

When YIG is introduced to this system, dark red, magnetic prisms formed in the 5-10 mole % B_2O_3 range. Clear, non-magnetic rhombohedra formed with 15-30% B_2O_3 in the solvent. Thus garnet does not appear to be a congruent stable phase for the bismuth borate system.

Elwell et al[21] reported on the bismuth barium borate system (J. Cryst Growth 16 (1972) 67-70). This system has the advantage that it is a glass. A eutectic at 23.4 BaO: 62.4 Bi_2O_3: 14.2 B_2O_3 with a temperature of 600°C could not be reproduced in our check of this sytem.

The use of certain solvents such as Na_2O - MoO_3[18] may result in lowered growth temperatures and consequently more Bi substitution. Until more evidence exists for such a result the top seeded growth of rods must be deferred.

I. Bulk BiYbIG Crystals

Several bulk crystals of BiYbIG were grown. The composition is estimated as $Bi_1Yb_2Fe_5O_{12}$. Several (110) platelets were polished to ~ 50 μm thickness, and domains were observed with Faraday rotation as large as ±90°. The domains were not uniform due to zoning and small inclusions in the bulk crystal. The use of bulk crystals, particularly those grown isothermally, seems to hold some promise.

[21] Elwell et al, J. Cryst. Growth 16 (1972) 67-70

SECTION III
DRIVE ELECTRONICS

A. Background

The inherent polar symmetry of the stripe domain grating suggests two modes of scans 1) azimuthal, and 2) radial. In the azimuthal scan mode, the domain pattern rotates at a constant rate and the domain width increments once per cycle. In the radial scan mode the domain spacing changes in a controlled fashion and once every sweep the domain angle changes. These two modes utilize all of the available spots in diffraction space. An optical system is used to convert the polar scan to an x-y, Cartesian raster. Such a system could be a mirror which is a parabola of revolution with the grating mounted at the focus and the recording film located concentric to the axis. The generation of the drive field is most easily accomplished in the azimuthal mode; the x and y coils are driven in quadrature with a sine wave which is slowly amplitude modulated. Thus, large reverse inductive spikes are avoided.

B. Drive Circuitry

1. Spinning Scan

As a starting point for the design of the light deflector electronics, low frequency Helmholtz coil drivers were designed. The prototype circuit served both as an interim demonstrator and as a foundation for further studies on specialized sweep circuitry. Figure 21 is a schematic of the Helmholtz coil drivers. A 380 Hertz sine wave was converted into two amplitude modulated quadrature sine waves that drove two sets of orthogonal Helmholtz coils. An oscilloscope photograph of the field space of the Helmholtz coils appears as an insert to Figure 21. Since the stripe domain sample is located in the field space of the Helmholtz coils it experiences the radially incremented spinning field.

2. Radial Sweep Scan

Further experimentation indicated that when the diffracted spots are initially at rest, 25 Oe of field is required to move the stripes out of the rest position. Once

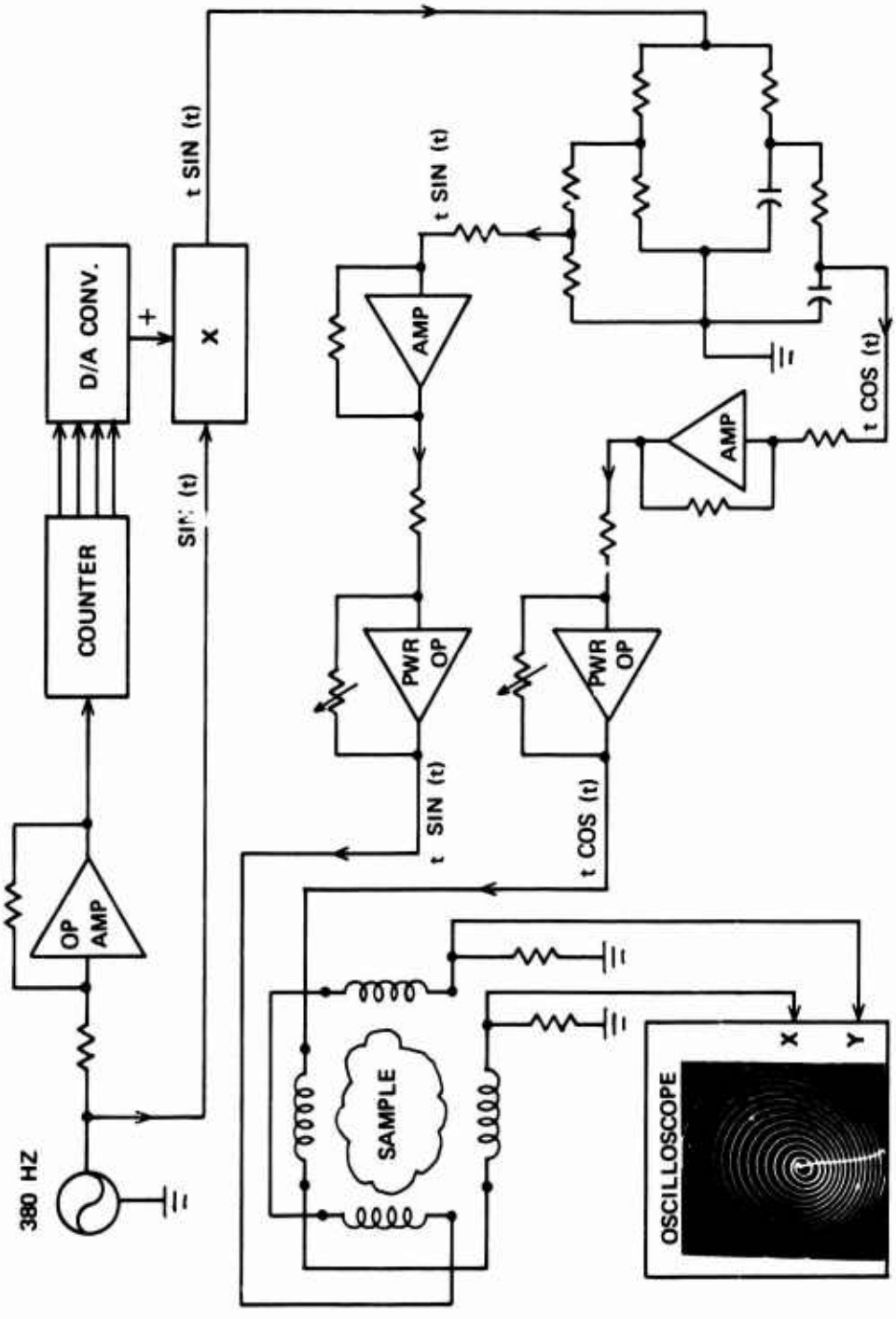

Figure 21. Circular Field Generator.

the stripes are moving they respond well to the spiralling field. Apparently the grating as a whole does not turn easily in the presence of small fields. However, if the film is brought to saturation and then returned to its rest position along a particular radial in field space the grating need not turn at all. For fields greater than saturation there are no domains but as the field sweeps down a radial a field point is reached where domain wall nucleation occurs. The walls nucleate parallel to the field and therefore there is no need to turn the grating before the next trace. The grating direction is inherently locked to the direction specified by that radial. As the field continues to drop toward 0 the grating spacing increases, thus diminishing the angle of diffraction. At 0 field the electronics retraces the field back to a value above saturation, increments the radius an angle ϕ and repeats the entire process as shown in Figure 22. The circuit of Figure 21 was modified to provide the type of field indicated in Figure 22. Figure 23 is a schematic of the modified circuit. The oscilloscope photograph insert to Figure 23 represents the field space as generated by the circuit. That field is constructed in the following manner. The counter clock input is switched off and the jam inputs are programmed for some desired maximum vector field value. Normally that would just provide a constant radius rotating field. However, at preset intervals field effect transistors gate off the coil drive electronics forcing the magnetic field to collapse to 0 along a radius. In the photo there are 20 such interrupts, each lasting but a fraction of the circumferential time and each exhibiting a high degree of linearity.

In order to achieve high speed linearity in a magnetic deflection coil it is necessary to account for the coil inductance, resistance and capacitance. Usually the capacitance is small enough to be ignored during the trace time and may or may not be ignorable during retrace time. Often a certain amount of capacitance is designed into a deflection coil in order to obtain a resonant type retrace mode. In the following analysis the stray capacitance is disregarded. Refer to Figure 24, an LR circuit with waveforms pertinent to this discussion. The question to be answered is, what kind of forcing function e(t) is required to produce a current sawtooth in the LR circuit? The analysis will show that function to be a trapezoidal waveform.[22] Consider first the inductance L. During the trace time the circuit

[22]Fink, Television Engineering.

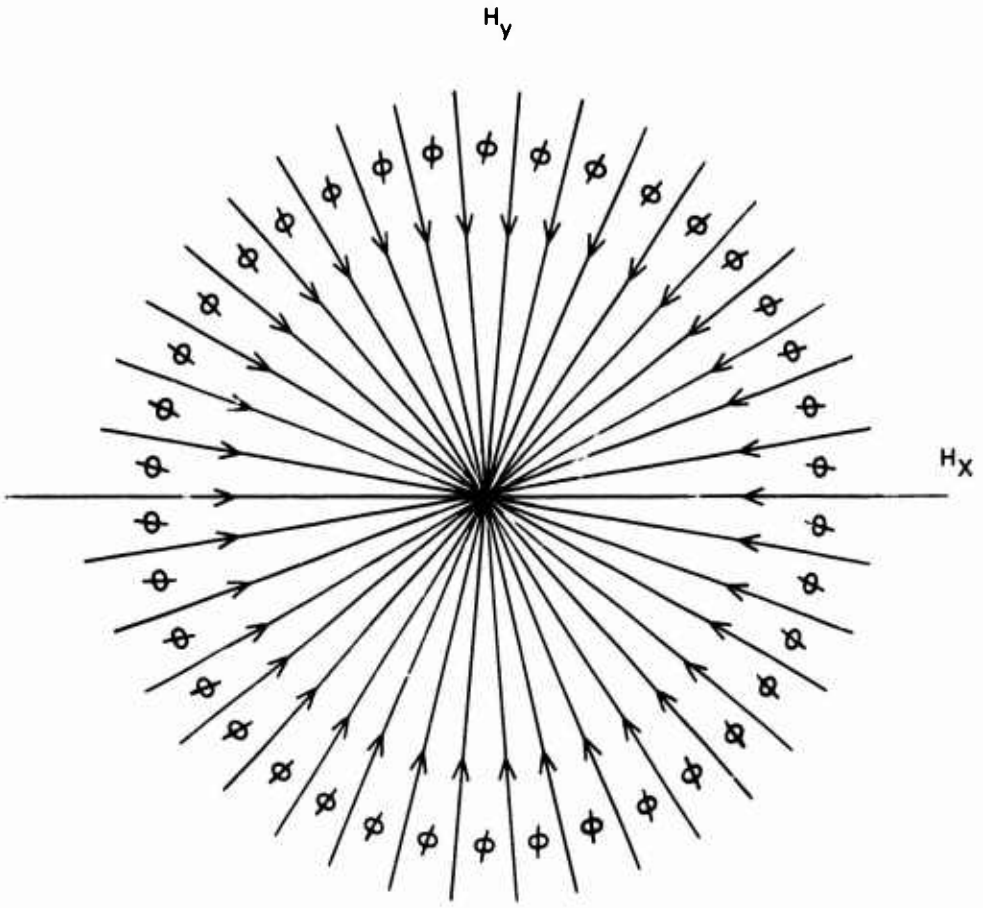

Figure 22. Radially Scanned Field.

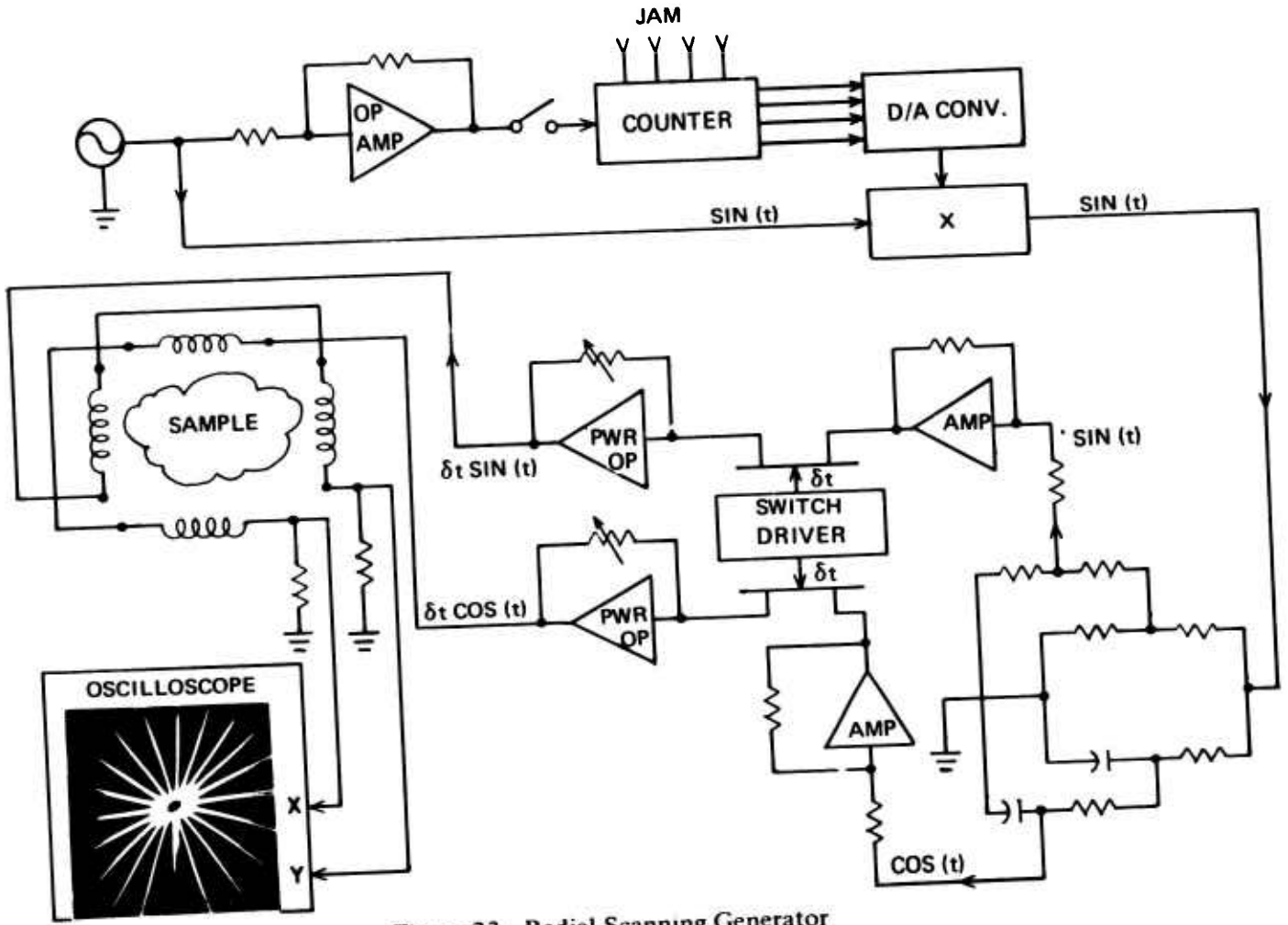

Figure 23. Radial Scanning Generator

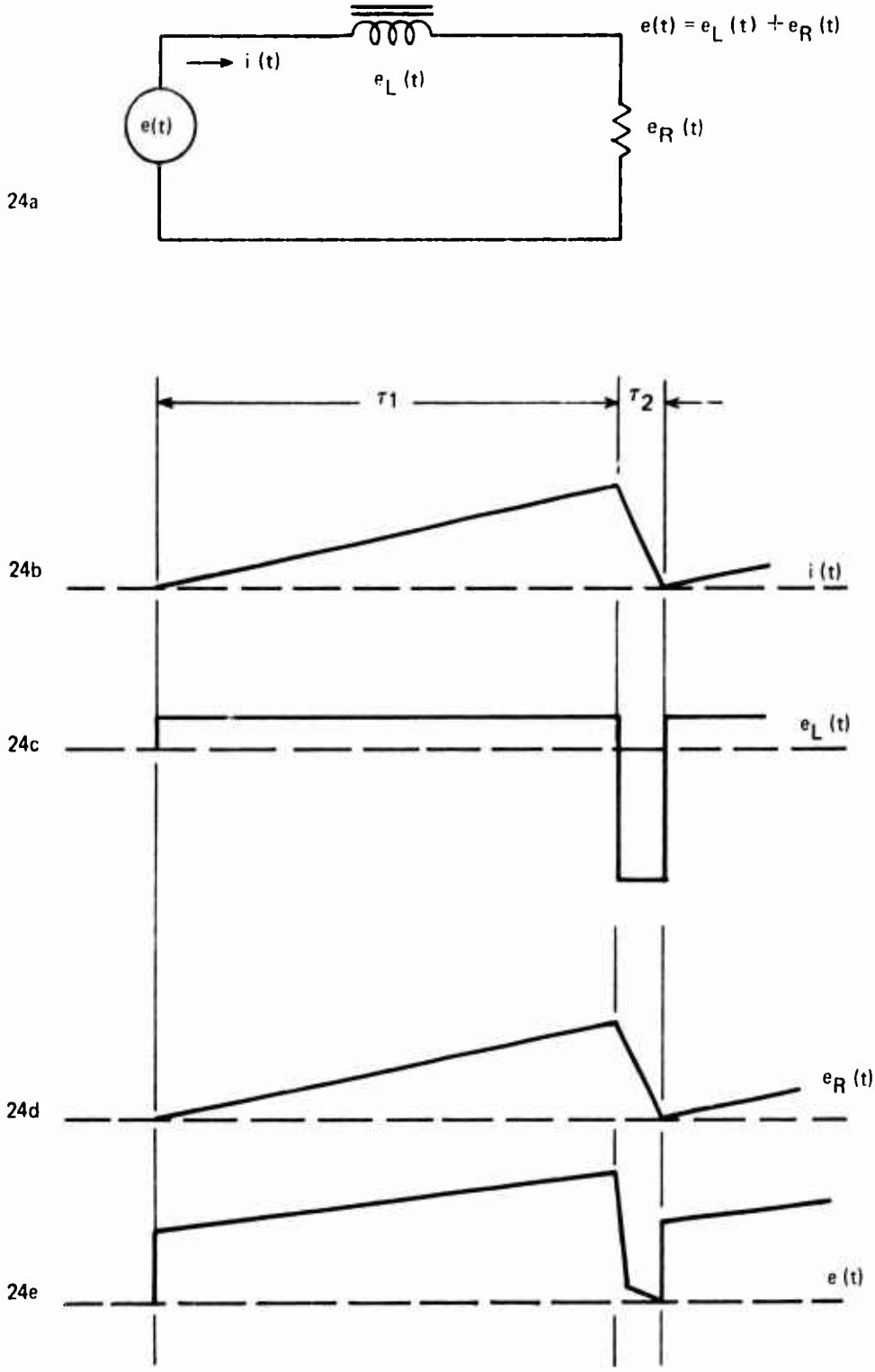

Figure 24. LR Circuit

current is i = At for a sawtooth where A is the slope of the ramp $\left(\frac{\Delta I}{\tau_1}\right)$, a constant for any given ramp. The voltage across the inductance is

$$e_L = L\frac{di(t)}{dt}.$$

Substituting At for i(t) gives

$$e_L = L\frac{dAt}{dt} = LA.$$

Therefore E_L is a constant voltage and the higher the slope $\left(\frac{\Delta I}{\tau_1}\right)$ or the higher the inductance L, the greater the applied voltage must be to meet the ramp requirements. During retrace the same analysis applies but with $A = \frac{\Delta I}{\tau_2}$ instead of $\frac{\Delta I}{\tau_1}$. However $\tau_2 << \tau_1$ so that the retrace voltage must be much greater in magnitude than the trace voltage. The reactive voltages required to produce the trace and retrace currents are of opposite polarity and follow each other in time as shown in Figure 24c. The resistive part of the circuit satisfies the equation

$$e_R = i(t)\ R$$

and will follow the ramp current as shown in Figure 24d. Superposition of the reactive voltage e_L and the resistive voltage e_R produces the trapezoidal forcing function of Figure 24e.

Any television circuit designer knows how to generate a trapezoidal waveform. Figure 25 is a typical method. During the trace time, τ_1, transistor Q is turned off and capacitor C charges up to approximately $\frac{Vcc}{5}$ through resistors R_p and R_1. At retrace time the transistor throws a short across R_p and C forcing C to rapidly discharge. If the R_pC time constant is made equal to the $\frac{L}{R}$ time constant of the coil driven by the circuit, an essentially linear current ramp in the LR circuit results.

The saturated switch method of the last paragraph works well enough if Vcc is a constant voltage, but not at all when Vcc is a time varying voltage. If the retrace has to jump to some large positive or negative value of voltage the circuit also fails to function properly. Now, in the light deflector coils, the current must sweep linearly from a magnitude greater than the crystal's saturation value down to zero

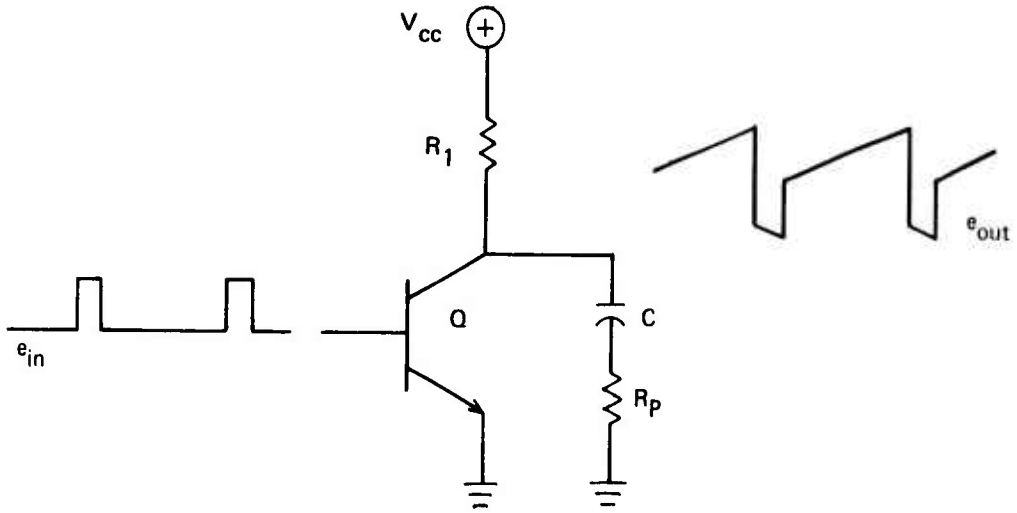

Figure 25. Conventional Trapezoid Generator

and then rapidly retrace back out to the saturation magnitude for angular incrementation. To accomplish this, a new trapezoidal generator circuit had to be designed that would both admit a low frequency modulation and provide for rapid retrace out to some voltage. Figure 26 is the result of that design effort. The two field effect transistors are used as analog gates. During retrace Q_2 is on and Q_1 is off and C charges up to the instantaneous value of the 30 cps modulating voltage. During retrace Q_1 turns on, Q_2 turns off, and the capacitor begins to discharge toward ground producing the trace portion of the cycle. Trace time is again followed by a retrace, but this time to a slightly different instantaneous voltage and the cycle repeats itself. In this manner a modulated trapezoidal voltage is produced.

Figure 27 is a schematic of a circularly modulated trapezoidal carrier circuit. Also in Figure 27 are oscilloscope photographs of salient voltages in the circuit. When this circuit is connected to a yet to be designed power amplifier it will be possible to generate a magnetic field that sweeps from some large value down to near ground in 35 μsec and then retraces back up to that large field value in approximately 2 μsec. Each retrace is followed by an angular increment and hence 360° of field space can be scanned in a rosette fashion.

3. Semicircle Radial Scan

Magneto-optic light deflector crystals inherently produce 2 diametrically opposed beams. Although there are optical methods available to combine the 2 beams it seemed reasonable to think about a semicircular field generator in the event that optical recombination be undesirable. This would keep one beam from scanning territory already scanned by the other beam when the system is driven with a full circle of field. One obvious way of generating a semicircular field is to generate a full circle of field and gate it off 50% of the time. This wastes system time and a more efficient method was investigated. Figure 28 is the block diagram of a prototype system that produces a radially scanned semicircular magnetic field.

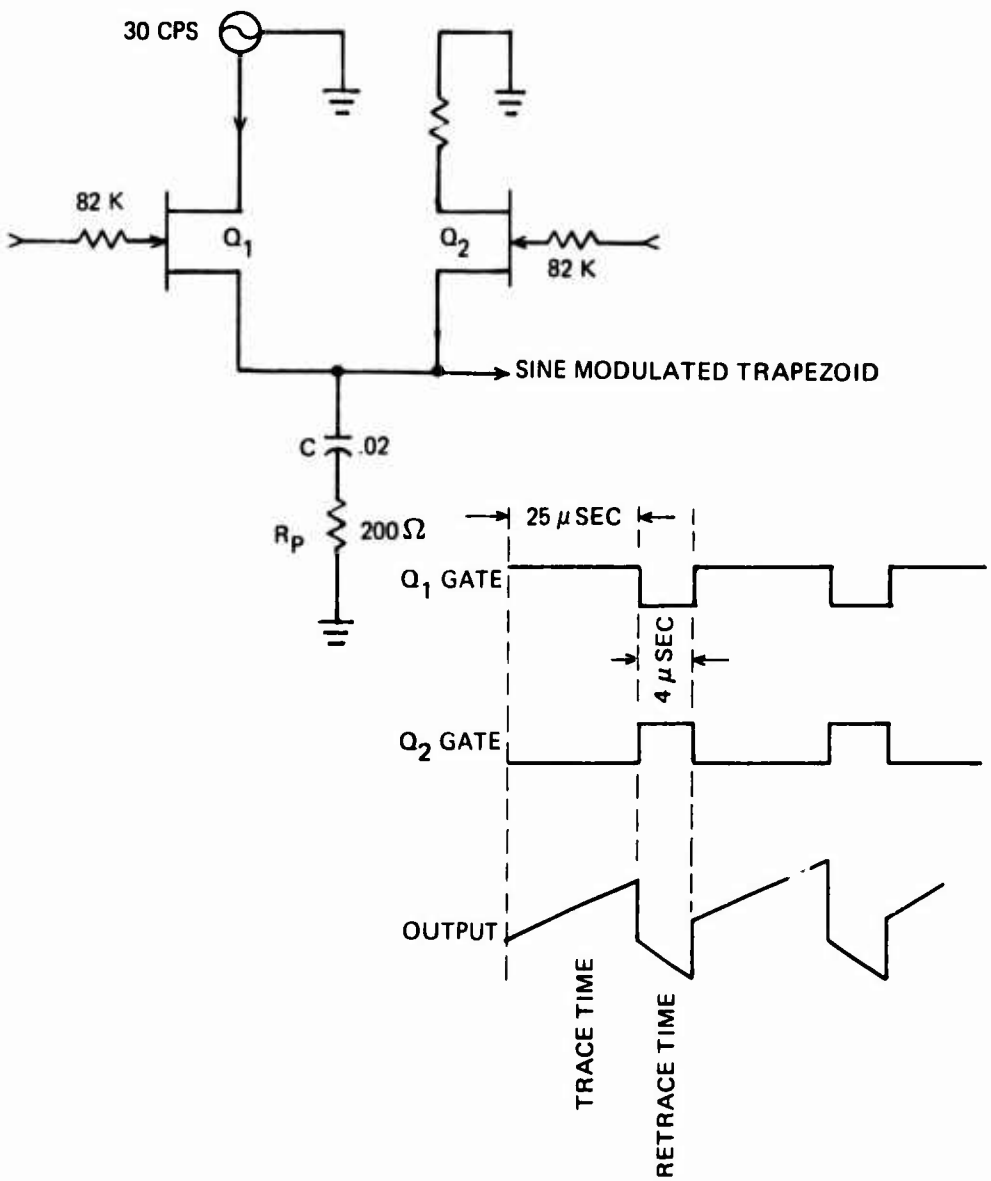

Figure 26. Sine Modulated Trapezoid Generator

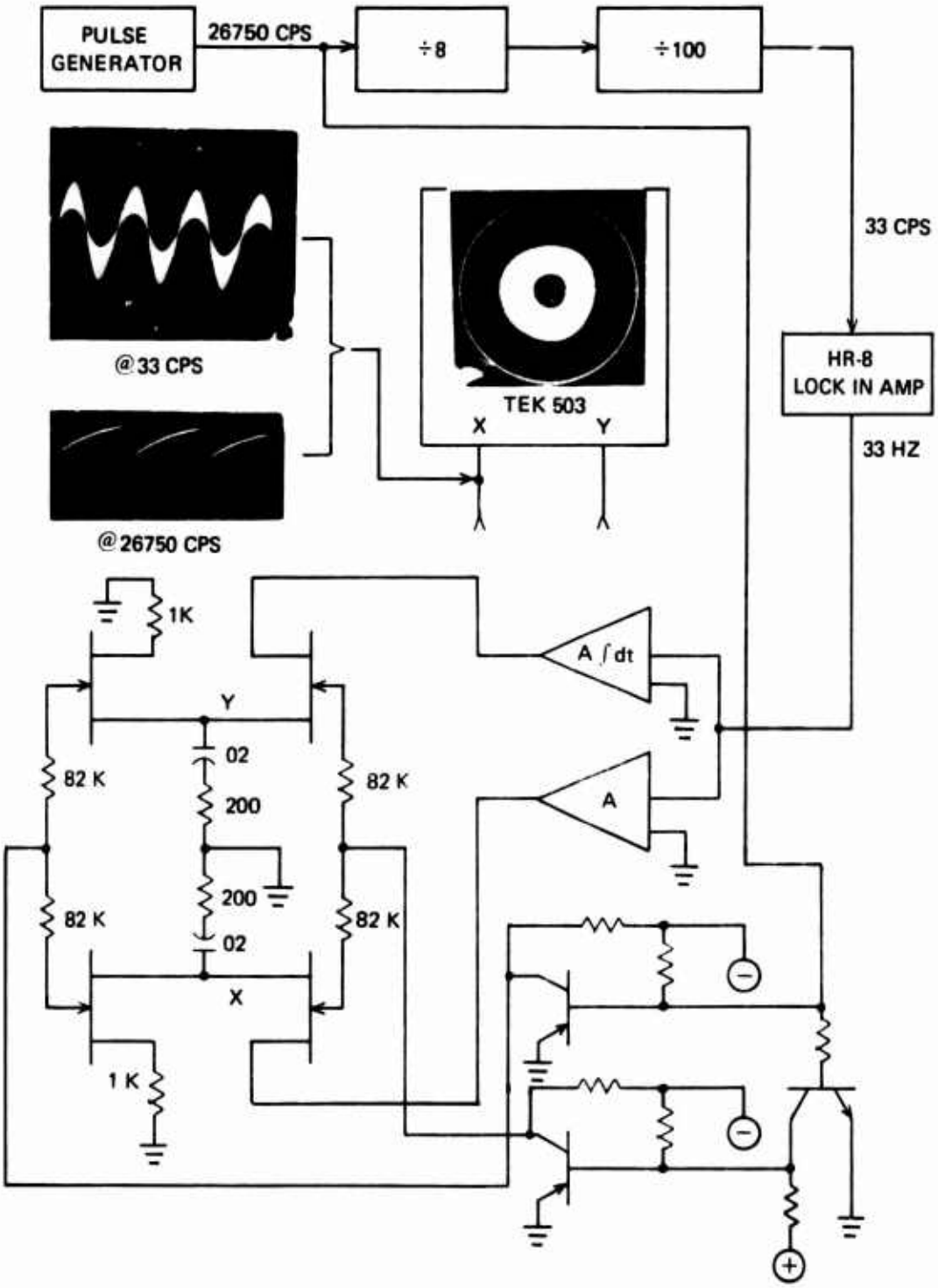

Figure 27. Circularly Modulated Trapezoid Generator

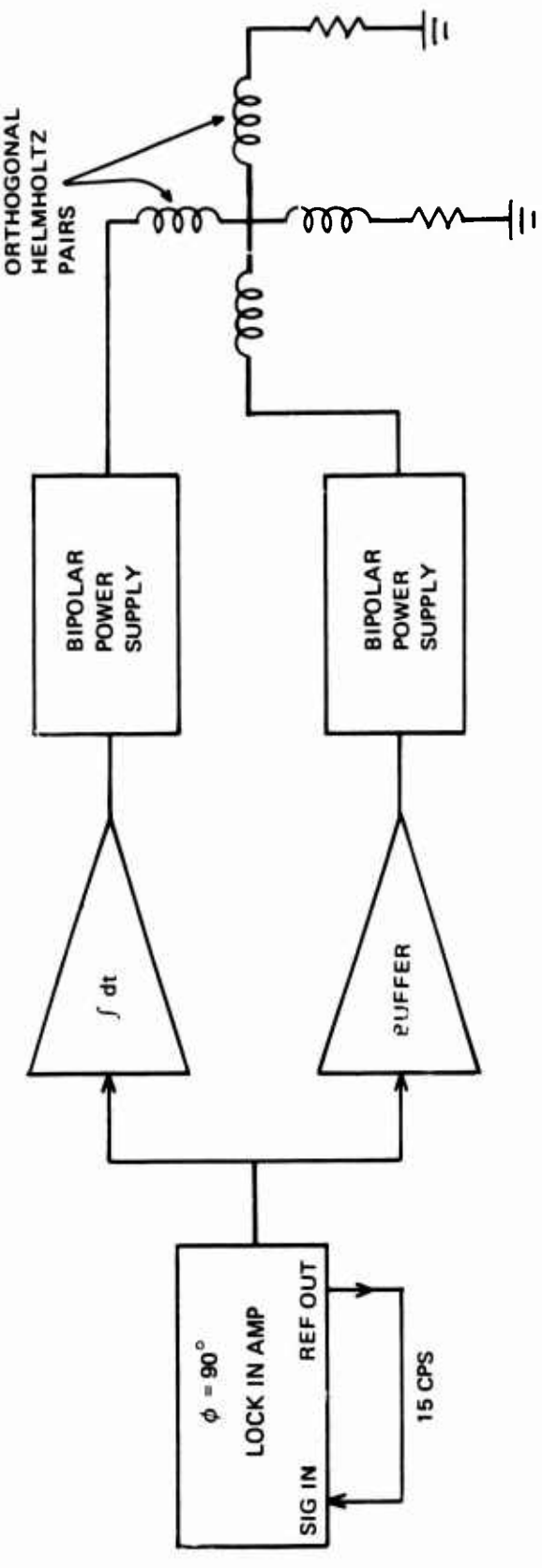

Figure 28. Semicircle Generator

It was known that in order to make a semicircular magnetic field in Cartesian coils the following parametric equations of the currents had to be satisfied.

$$x = I_o\,|\sin \omega t|,\ -\pi \le \omega t \le \pi$$

$$y = \begin{cases} I_o\,(-\cos \omega t),\ -\pi \le \omega t \le 0 \\ I_o\ \cos \omega t\ ,\ 0 \le \omega t \le \pi \end{cases}$$

X is essentially the output of a full wave rectifier while Y can be recognized as the unfiltered output of a phase detector that has the reference port in quadrature with the signal port. In Figure 28 the lock in amplifier was utilized as the phase detector to generate the Y axis signal directly. One integration of the Y signal produced the X axis signal. The following analysis will show that the integration of the Y signal yields the X signal. Consider the 2 functions f(t) and g(t) with

$$f(t) = |\sin \omega t|,\ -\pi \le \omega t \le \pi$$

$$g(t) = \begin{cases} -\cos \omega t,\ -\pi \le \omega t \le 0 \\ \cos \omega t,\ 0 < X \le \pi \end{cases}$$

The Fourier series of f(t) is

$$f(t) = \frac{2}{\pi} - \frac{4}{\pi} \sum_{n=1}^{\infty} \frac{\cos 2n\ \omega t}{4n^2 - 1}$$

The Fourier series of g(t) is

$$g(t) = \frac{8}{\pi} \sum_{n=1}^{\infty} \frac{n \sin 2n\ \omega t}{4n^2 - 1}.$$

One time integral of g(t) gives

$$\frac{8}{\pi} \int \left[\sum_{n=1}^{\infty} \frac{n \sin 2n\ \omega t}{4n^2 - 1} \right] dt =$$

$$= \frac{8}{\pi} \sum_{n=1}^{\infty} \int \left[\frac{n \sin 2n\,\omega t}{4n^2 - 1} \right] dt \text{ if}$$

uniform convergence is applicable except perhaps at jump discontinuities where Dirichlet conditions apply. Carrying out the integration for any n gives

$$\int \frac{n \sin 2n\,\omega t\, dt}{4n^2 - 1} = - \frac{n \cos 2n\,\omega t}{2n\,\omega\,(4n^2 - 1)} + C_n.$$

Substituting back into the summation gives

$$- \frac{8}{\pi} \sum_{n=1}^{\infty} \frac{\cos 2n\,\omega t}{2\omega\,(4n^2 - 1)} + C_n$$

$$= \frac{-4}{2\pi f \pi} \sum_{n=1}^{\infty} \frac{\cos 2n\,\omega t}{4n^2 - 1} + C_n = \int g(t)\, dt.$$

This is essentially equal to f(t) except for 2 things: 1) a d.c. offset term that can be eliminated by capacitive coupling and 2) the factor $\frac{1}{2\pi f}$. That factor is a function of the fixed fundamental frequency of the system and hence is a constant. The factor can be unitized by passing the signal through an amplifier of gain $2\pi f$. Figure 29 contains photographs of the waveforms existing in the radially incremented semicircle generator. The photograph of the polar coordinate scan shows the aforementioned d.c. offsets. These were not capacitively blocked because it was more important to preserve the low frequency response of the system.

During the investigations on electronic circuits it was observed that sample 5D1 contains what appears to be low coercivity anomalies. Portions of the diffracted beam move in response to much smaller fields than the main part of the beam. The effect can be observed only when the laser light is focused to a very small point on the sample. Fields as low as 3.8 oersteds were sufficient to observe this anamolous behavior. Although this is only a recent discovery it is hoped that further investigations of this phenomenon will be fruitful. Low in plane coercivity films would be ideal. Until low coercivity films can be easily fabricated it will be necessary to continue to search for indirect methods of accurately controlling grating orientation.

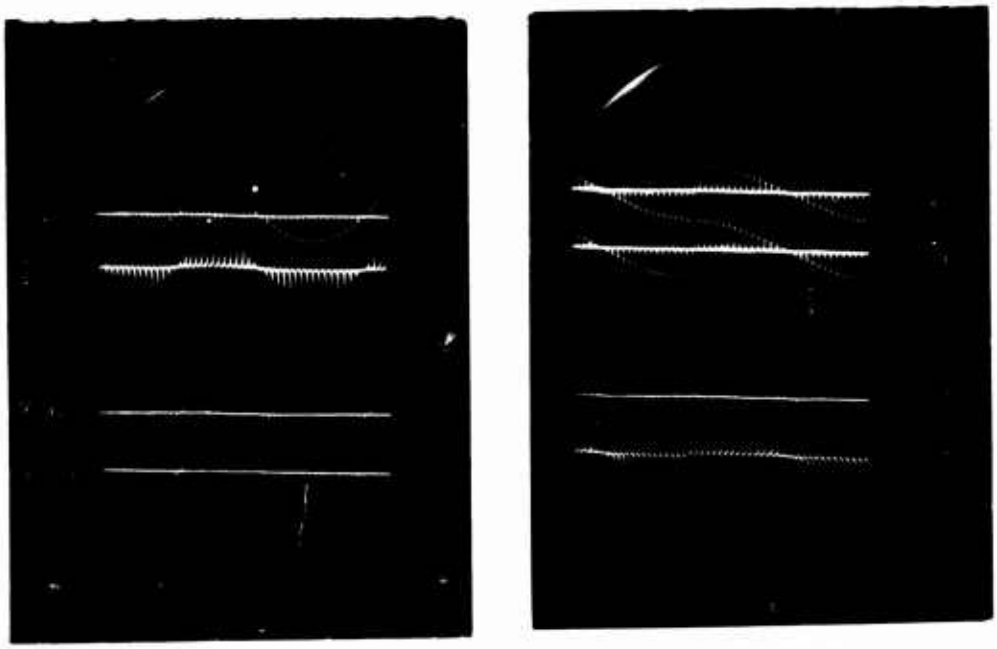

X AXIS COILS

Y AXIS COILS

POLAR REPRESENTATION

Figure 29.

4. RF Drive Scan Assist

In September of 1973 a paper[23] appeared that reported on resonant stripe domain steering in thin films of $(Y\ Gd)_3(Fe\ Ga)_5\ O_{12}$. The eport shows that stripe domains line up underneath a coplanar transmission line that is driven at the ferrimagnetic resonant frequency (1-2 GHz) of the material. Although that report concentrates on magnetic bubble detection it does indicate the feasibility of stripe domain steering by the resonance mechanism.

It is helpful to know a priori the approximate frequency needed to achieve the resonant condition in a particular sample. That frequency is available from the following formula:

$$\omega_r = \left| \frac{\gamma}{2\pi} (H_{app} - 4\pi M_{sat} + H_k) \right|$$

where γ = gyromagnetic ratio = $\frac{2.8\ MHz}{Oe}$.

H_{app} = an applied dc bias field

M_{sat} = saturation magnetization

H_k = anisotropy field (induced and/or magnetocrystalline).

Sample #305 ($(TmBi)_3(FeGa)_5O_{12}$ on a GGG substrate) was selected for a stripe steering experiment. By Faraday rotation $-4\pi M_{sat} + H_k$ was found to be -50 oersteds. Using 50 Oe and no dc bias ω_r was computed to be 139 MHz in the above equation. With this frequency in mind a coplanar transmission line system was constructed in the manner of Figure 30, and placed in the experiment of Figure 31. An rf driven coplanar line yields elliptically polarized magnetic fields in the plane of the line and also in the plane of a sample placed on top of the line.[24] With r.f. currents as high as .5 amp peak we were unable to detect any motion of the stripe domains or to see any indication of energy absorption at 139 MHz. Other

---

[23]Dotsch, Stal. Appl. Phys. Lett. - Vol. 23, 11 (1973)

[24]Wen, IEEE Trans Microwave MTF17 (1969) 1087

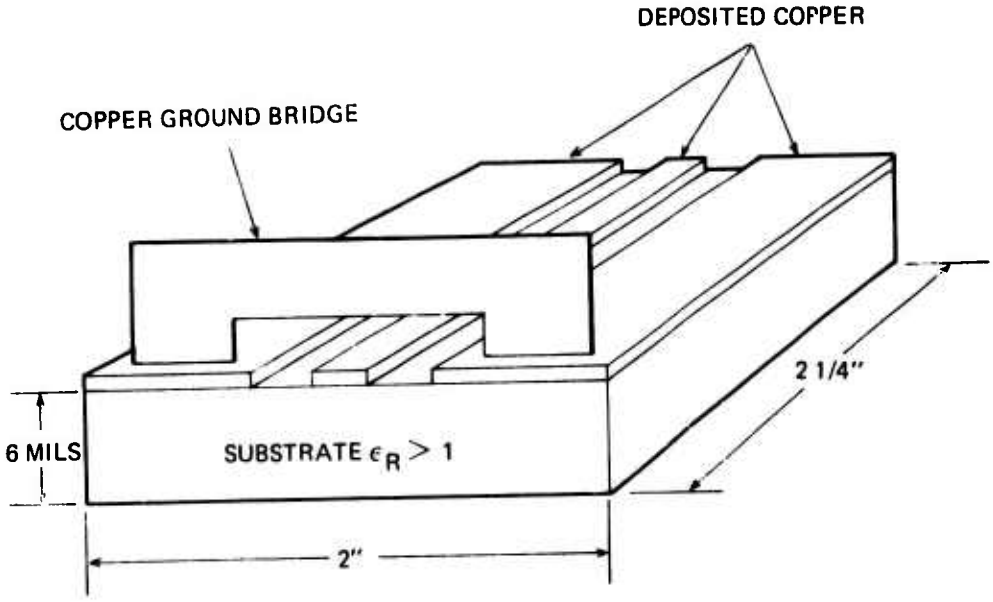

Figure 30. Coplanar Transmission Line

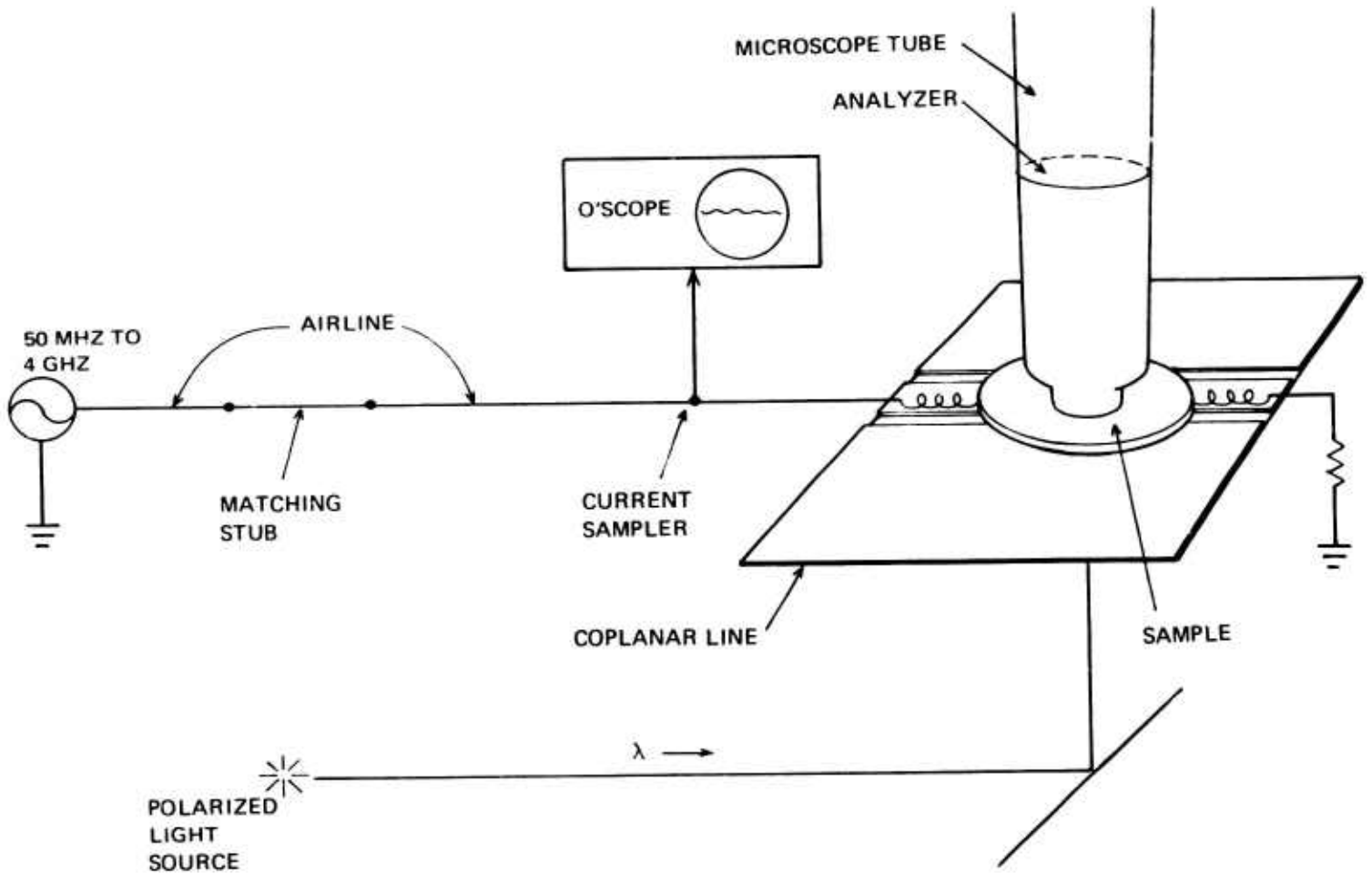

Figure 31. Ferrimagnetic Resonance Apparatus

frequencies (50 MHz to 4 GHz) were equally disappointing. At this time it is not known why the resonance mode was not seen. Some possibilities, though, are:

1) the rf magnetic fields were not elliptically polarized;

2) sample Q too high or too low;

3) high coercivities that require large fields to overcome;

4) demagnetizing fields.

C. Scan Control Module

During the latter part of the contract period a Scan Control Module and a coil assembly were designed and built. Figure 32 is a block diagram of the SCM. A 3 Kc. TTL type pulse is converted into separate 30 Hz. sine and cosine voltages that are chopped 20 times each cycle. The chopped voltages are coupled into Kepco Bipolar Operational power supplies that source the current for the field coils. Initial tests on the system using sample 5D1 have been encouraging.

Deflection angle as a function of applied field was measured on sample 5D1. The light source was a 6328Å He-Ne laser. Figures 33 and 34 are graphs of the results of the measurements. Each graph contains a curve for static field deflection and a curve for dynamic field deflection. The static field curve was made by applying a d.c. field and recording the deflection angle as the field was slowly increased. The dynamic curve was made by applying an alternating field that was generated by the deliverable electronics to the sample and measuring the width of the deflection trace as the peak to peak magnitude of the field was slowly increased. Although the curves show a maximum deflection angle of about 800 milliradians, deflections of one radian have been occasionally observed.

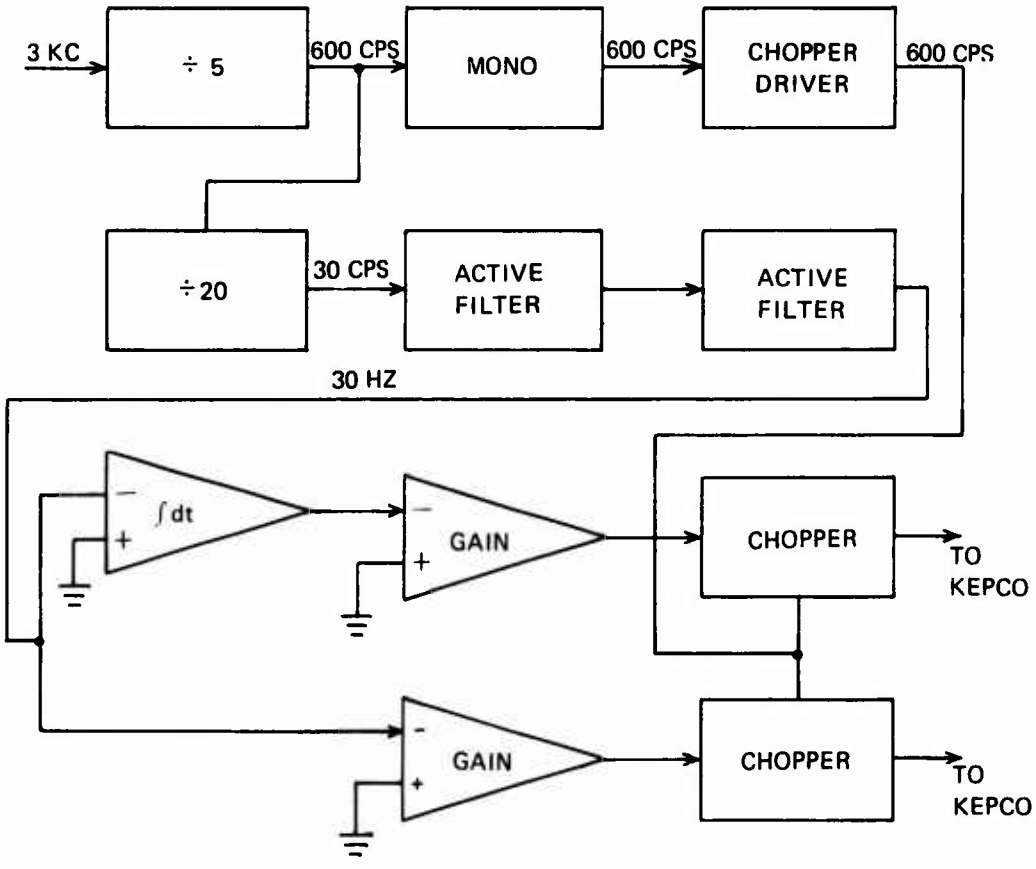

Figure 32. Scan Control Module

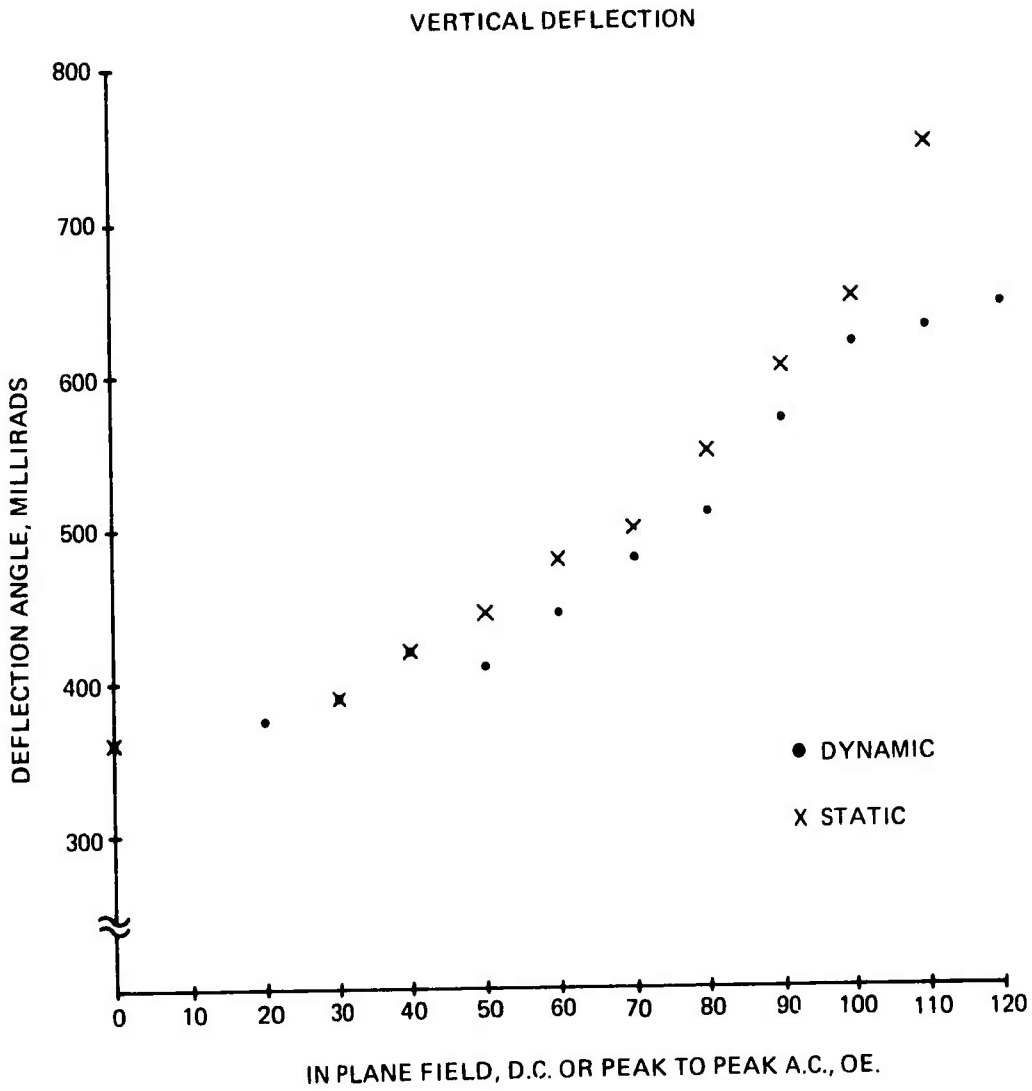

Figure 33. Angle vs. Drive

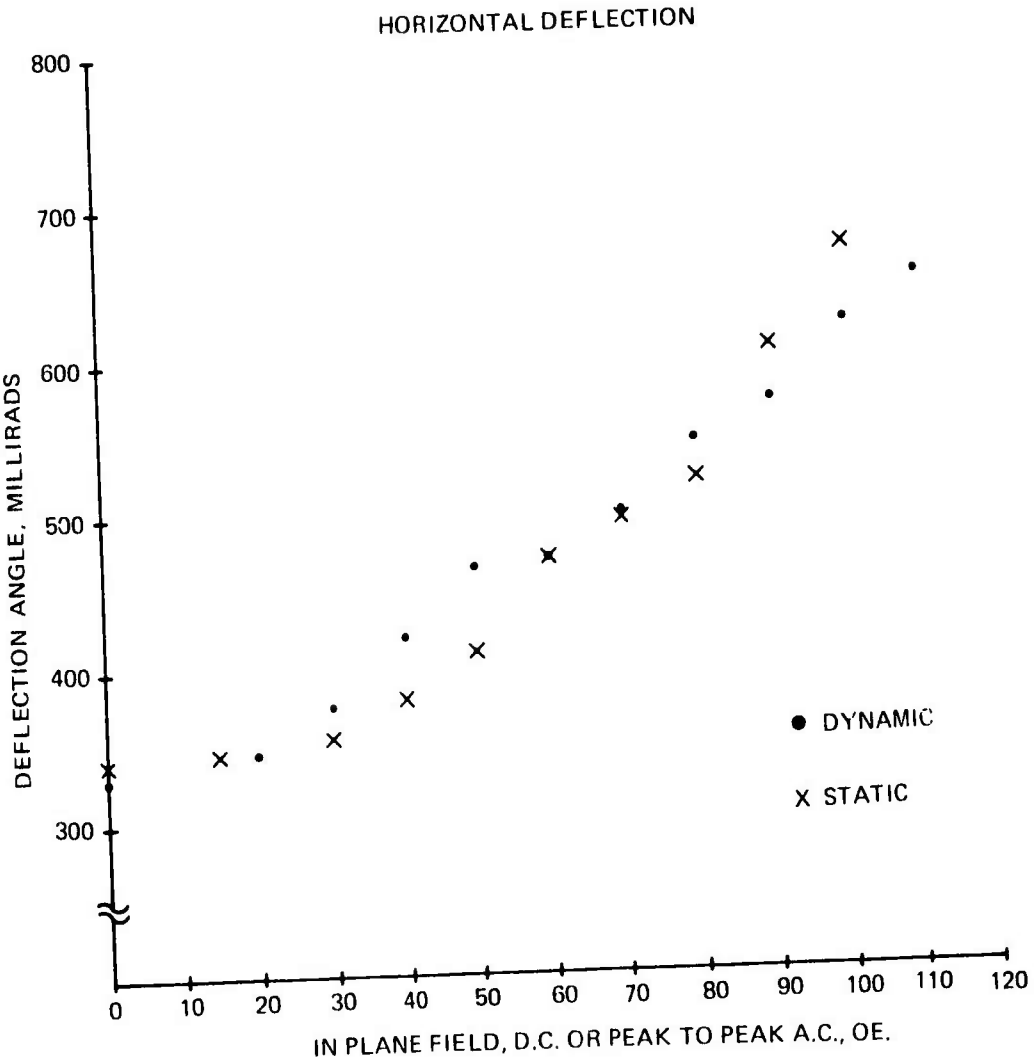

Figure 34. Angle vs. Drive

SECTION IV
CONCLUSIONS AND RECOMMENDATIONS

The stripe domain light deflector continues to promise great advantages over existing devices such as acousto-optic deflectors. A single stage x-y stripe domain deflector for example could ultimately offer two orders of magnitude more resolvable spots than a two stage acousto-optic deflector. However, at present, there are material problems.

The scan capability of the magneto-optic laser beam steering device at this point in time mirrors the level of development of the BRIG crystal. The azimuthal coercivity of the crystal has not yet been made low enough to use an azimuth scan and at the same time utilize all of the spots in the diffraction space. The drive field required to initiate an azimuth scan is about 30 Oe. The normal direction anisotropy field has not yet been made small enough to use a radial scan in conjunction with low-inductance (micro-henry) drive field coils. As a result the practical number of lines at 30 frames/sec is between 50 and 100 lines whereas the design goal is 875 lines. The number of spots per line is about 300.

The problem associated with the fabrication of BRIG crystal element has been identified. The thermal expansivity of BRIG does not match the expansivity of the substrate crystals. As a result, if an epitaxial BRIG crystal grows with a perfect in-plane lattice match, it will develop enough tensile strain to cause fracturing and to cause a large normal strain induced anisotropy. If the crystal does not have a perfect in-plane match, the misfit dislocations will diminish its usefulness by causing large coercivity.

Several alternative crystal fabrication approaches were probed and one method, LPE on thin substrates, appears to offer an excellent short term solution to the problem. All of the component steps in this approach have been demonstrated, save perfect in-plane match verification. The best long term solution is to find a way to improve the thermal match.

It is our recommendation that the BRIG crystal problem be given an intensive treatment. There is every reason to believe that excellent BRIG crystals can be obtained and that with these crystals every device goal of the laser recorder could be met or surpassed.

REFERENCES

[1]Technical Report AFAL-TR-72-396

[2]Technical Report AFAL-TR-74-183

[3]Besser et al, AIP Conf. Proc. No. 5 (1971) p 125

[4]Geller et al, J. Appl. Cryst, Vol. 2 (1969) 86

[5]Geller et al, Mat. Res. Bull., Vol. 7 (1972) 1219

[6]Besser et al, Mat. Res. Bull. 6 (1971) 1111-1124

[7]Makino et al, AIP Conf. Proc., No. 18 (1973) 80

[8]Robbins et al, AIP Conf. Proc., No. 5 (1971) 101

[9]Cronemeyer et al, AIP Conf. Proc., No. 5 (1971) 115

[10]Matthews et al, AIP Conf. Proc., No. 10 Part 1 (1972) p 271

[11]Laudise and Kolb, J. Am. Cer. Soc., Vol. 45, 2 (1962) 51

[12]Ferrand and Daval, J. Cryst. Growth, Vol. 17 (1972) 312

[13]Miller, J. Elect. Matls., Vol. 1, 4 (1972)

[14]Miller, Electro Chem. Soc., Vol. 120, 5 (1973) 678

[15]Sturge et al, Matl. Res. Bull., Vol. 7 (1972) 989-998

[16]Lineras, J. Appl. Phys. 35, 2 (1964) 433

[17]Kestigian, J. Am. Ceram. Soc. 50, 3 (1967) 165

[18]Lineras, J. Am. Ceram. Soc., 45, 7 (1962) 307

[19]Geller et al, Appl. Phys. Letter, 3, 2 (1963) 21

[20]Levin et al, Phase Dia. Ceram., Am. Cer. Soc. 1964

[21]Elwell et al, J. Cryst Growth, Vol. 16 (1972) 67

[22]Fink, Television Engineering

[23]Dotsch et al, Appl. Phys. Letter, Vol. 23, 1 (1973)

[24]Wen, IEEE Trans Microwave MT F17 (1969) 1087